Published in final edited form as:
Nature. 2019 May 01; 569(7755): 284–288. doi:10.1038/s41586-019-1141-3.

Structural insights into lipid and ligand regulation of serotonin receptors

Peiyu Xu[#1,2,3], **Sijie Huang**[#2,3,4], **Huibing Zhang**[#5,6,7], **Chunyou Mao**[#1,5,6,7], **X. Edward Zhou**[#8], **Xi Cheng**[#9], **Icaro A. Simon**[11,12], **Dan-Dan Shen**[1,6,7], **Hsin-Yung Yen**[13], **Carol V. Robinson**[13], **Kasper Harpsøe**[12], **Bo Svensson**[12], **Jia Guo**[2,3], **Hualiang Jiang**[9], **David E. Gloriam**[11], **Karsten Melcher**[8], **Yi Jiang**[2,†], **Yan Zhang**[1,5,6,7,†], **H. Eric Xu**[2,3,4,†]

[1]Department of Biophysics, and Department of Pathology of Sir Run Run Shaw Hospital, Zhejiang University School of Medicine, Hangzhou 310058, China

[2]The CAS Key Laboratory of Receptor Research, Shanghai Institute of Materia Medica, Chinese Academy of Sciences, Shanghai 201203, China

[3]University of Chinese Academy of Sciences, Beijing 100049, China

[4]School of Life Science and Technology, ShanghaiTech University, 201210 Shanghai, China

[5]Zhejiang Laboratory for Systems & Precision Medicine, Zhejiang University Medical Center, Hangzhou 311121, China

[6]MOE Frontier Science Center for Brain Research and Brain-Machine Integration, Zhejiang University School of Medicine, Hangzhou 310058 Zhejiang, China

[7]Key Laboratory of Immunity and Inflammatory Diseases of Zhejiang Province, Hangzhou 310058, China

[8]Center for Cancer and Cell Biology, Program for Structural Biology, Van Andel Institute, Grand Rapids, MI 49503, USA

[9]State Key Laboratory of Drug Research and CAS Key Laboratory of Receptor Research, Shanghai Institute of Materia Medica, Chinese Academy of Sciences, Shanghai 201203, China

[†]Correspondence: yijiang@simm.ac.cn (Y.J.), zhang_yan@zju.edu.cn (Y.Z.), eric.xu@simm.ac.cn (H.E.X.).

Author contributions

P.X. and S.H. designed the expression constructs, purified the complexes, prepared samples for negative stain and data collection toward the structures, and prepared the figures and manuscript draft. P.X., H.Z., C.M., and D.-D.S. evaluated the specimen by negative-stain EM, screened the cryo-EM conditions, prepared the cryo-EM grids, collected cryo-EM images, processed the cryo-EM data, and participated in the preparation of supplementary figures. X.E.Z., P.X., and H.Z. built the models and refined the structures. I.S. and K.S.H. conducted analyses of ligand-receptor structure-activity relationships and contributed to writing. K.S.H. performed data curation of mutagenesis data. B.S. and D.E.G. were responsible for the funding and supervision of I.A.S. and K.H., and participated in writing. X.C. and H.J. were responsible for molecular dynamics simulation studies, ligand docking studies and writing of methods. K.M. supervised X.E.Z. and participated in writing. H-Y.Y. and C.V.R. analyzed lipids composition and edited the manuscript. Y.J. participated in the supervision of P.X. and S.H., fund acquisition, and paper editing. Y.Z. supervised the cryo-EM data collection, data analysis, and participated in writing. H.E.X. conceived and supervised the project, analyzed the structures, and wrote the manuscript with inputs from all authors.

Competing interests: The authors declare no competing interests.

Europe PMC Funders Author Manuscripts

[11]Department of Drug Design and Pharmacology, University of Copenhagen, Universitetsparken 2, 2100 Copenhagen, Denmark

[12]SARomics AB Biostructures, Scheelevägen 2, 223 63 Lund, Sweden

[13]Physical and Theoretical Chemistry Laboratory, University of Oxford, South Parks Road, Oxford OX1 3QZ, UK

[#] These authors contributed equally to this work.

Abstract

Serotonin, or 5-hydroxytryptamine (5-HT), is an important neurotransmitter[1,2] that activates the largest family of G-protein coupled receptor subtypes[3]. Drugs targeting serotonin receptors, including 5-HT_{1A}, 5-HT_{1D}, and 5-HT_{1e}, are used for numerous disorders[4]. In addition, serotonin receptors have high basal activation and are subject to lipid regulation, but the structural basis for lipid regulation, basal activation, and serotonin pan agonism remains unclear. Here we report five structures of serotonin receptor-G protein complexes: three 5-HT_{1A} complexes either in the apo state, bound to serotonin, or bound to the antipsychotic drug, aripiprazole; one 5-HT_{1D} complex with serotonin and one 5-HT_{1e} complex with a 5-HT_{1e} and 5-HT_{1F} selective agonist, BRL-54443. Unexpectedly, phospholipid PI4P was found at the interface of 5-HT_{1A} with G-protein and is able to increase 5-HT_{1A}-mediated G-protein activity. The receptor transmembrane domain is surrounded by cholesterols, particularly at 5-$HT_{1A,}$ where cholesterols are directly involved in shaping the ligand pocket that determines the aripiprazole specificity. Within the apo 5-HT_{1A} ligand-binding pocket are structured water molecules that mimic 5-HT to activate the receptor. Together, these results address a long-standing question of how lipids and water molecules regulate GPCRs and reveal the basis for pan agonism of serotonin and determinants of drug recognition of serotonin receptors.

The pleiotropic functions of 5-HT are in part mediated through 12 different subtypes of G protein-coupled receptors (GPCRs), which are regulated by a variety of factors, including ligands and lipid molecules[5]. Phospholipids and cholesterol are known to bind GPCRs to modulate their activity[6,7]. Three major phosphoinositides are phosphatidylinositol (PI), phosphatidylinositol 4-phosphate (PI4P), and phosphatidylinositol 4,5-bisphosphate [$PI(4,5)P_{2,}$ or PIP_2][8]. PI4P is the precursor of PIP_2 and was reported as a major mediator of GPCR-stimulated production of the second messenger, diacylglycerol (DAG)[9]. In addition, various types of phosphoinositides have been reported to bind GPCRs and regulate their activities[10,11], but the lack of structural information limits the mechanistic understanding of the exact types of phosphoinositides and how they regulate GPCRs.

Many GPCRs also exhibit intrinsic basal activity in the apo state[12,13], including 5-HT receptors[14], whose high basal activities are required for their normal physiological functions and inhibition of these basal activities by inverse agonists causes adverse effects[15]. 5-HT_{1A}, 5-HT_{1D}, and 5-HT_{1e} are among the 5-HT receptors that are primarily coupled to $G_{i/o}$. 5-HT_{1A} is the prototype serotonin receptor that exhibits high basal activity and is subjected to lipid regulation[14,16]. 5-HT_{1A} ligands, including aripiprazole, have been used to treat many CNS diseases such as schizophrenia and depression. 5-HT_{1D} exhibits high sequence homology with 5-HT_{1B} and they are the primary targets of the triptan class of antimigraine

drugs[17]. 5-HT_{1e} is expressed in brain regions important for memory[18]. No structure of 5-HT_{1A}, 5-HT_{1D}, and 5-HT_{1e} has been reported. In this paper we report five cryo-EM structures of serotonin receptor-G_i complexes, including three 5-HT_{1A} structures, in the apo state or bound to 5-HT and the aripiprazole; one 5-HT_{1D} structure bound to 5-HT, and one 5-HT_{1e} structure bound a 5-HT_{1e}- and 5-HT_{1F}- selective agonist BRL-54443. These results address a long-standing question of phospholipid regulation of GPCRs and reveal the basis for 5-HT pan-agonism and drug recognition at the serotonin receptor system.

Structures of 5-HT_{1A}, 5-HT_{1D}, and 5-HT_{1e}

We assembled serotonin receptor-G_i complexes by co-expression of the receptors with a dominant-negative human $G\alpha_{i1}$ [19] and human $G\beta\gamma$ (Extended Data Fig. 1a, b, 2a, b). The structures of the 5-HT_{1A}-G_i complexes in the apo state, or bound to 5-HT and aripiprazole, were determined at the resolution ranges of 3.0-3.1 Å. The structures of the serotonin-bound 5-HT_{1D}-G_i complex and the BRL-54443-bound 5-HT_{1e}-G_i complex were both determined at 2.9 Å (Fig. 1, Extended Data Fig. 1-2). The EM maps are sufficiently clear to define the position of the receptor, the G protein trimer, and the bound ligands in the receptor-G protein complexes (Fig. 1, Extended Data Fig. 1-2). The overall structures of 5-HT_{1A}, 5-HT_{1D}, and 5-HT_{1e} consist of a canonical transmembrane domain (TMD) of seven transmembrane helices (TM1-7), a short intracellular loop 2 (ICL2) helix, and an amphipathic helix H8 (Fig. 1b).

All three 5-HT receptors share a similar conformation, including a pronounced outward movement of TM6 at the cytoplasmic end relative to the inactive 5-HT receptor structures[20], a hallmark of GPCR activation. Although the overall structures of the three 5-HT receptor-G_i complexes are similar to that of the 5-HT_{1B}-G_o complex[21], several distinct features were observed. Compared to 5-HT_{1B}, 5-HT_{1A} and 5-HT_{1D} have helical extensions at the cytoplasmic end of TM6 (13 residues for 5-HT_{1A} and 9 residues for 5-HT_{1D}, Fig. 1c). 5-HT_{1D} has an additional 7-residue extension at the cytoplasmic end of TM5 as part of intracellular loop 3 (ICL3, Fig. 1c). These additional structural elements in 5-HT_{1A}, 5-HT_{1D}, and 5-HT_{1e} are close to the $G\alpha_i$-Ras domain and form extra interactions in the receptor-G protein complex assembly (Fig. 1c).

PI4P regulates the activation of 5-HT_{1A}

The most surprising observation in the three 5-HT_{1A}-G_i structures is a bound phospholipid at the interface between the receptor and the $G\alpha_i$ (Fig. 2, Extended Data Fig. 3a-e). The structures of 5-HT bound, aripiprazole-bound, and the apo-state 5HT_{1A} present a clear EM map that can be best fit with a PI4P molecule (Extended Data Fig. 3f). The two acyl chains with 14-16 visible carbons form extensive hydrophobic interactions with TM6 and TM7/H8 (Fig. 2a, b). The PI4P head group is inserted into a cavity formed between TM3/6/7 of the receptor and the α5 helix of G_i-protein (Fig. 2a, b, Extended Data Fig. 3d, e). The 4-phosphate group of PI4P forms a salt bridge with the conserved $R134^{3x50}$ of the receptor and a hydrogen bond with C351 of the $G\alpha_i$ (Fig. 2b, Extended Data Fig. 3e). The myo-inositol group interacts with the receptor residues $T346^{6x36}$, $K345^{6x35}$, $F403^{7x56}$, $N404^{8x47}$, $K405^{8x48}$, and with G352 of the $G\alpha_i$ protein (Extended Data Fig. 3e). We reasoned that the

binding of PI4P at the interface between 5-HT_{1A} and G protein might stabilize their complex formation. To test this hypothesis, we reconstitute 5-HT_{1A}-G_i (WT) complex to peptidiscs[22] with different lipids, in which the composition of lipids was defined. Then the GTPase-Glo assay was adopted to determine the effect of phospholipids on GPCR-mediated G protein activation, by measuring the GTP hydrolysis activity of G_i when coupled to 5-HT_{1A} in the presence or absence of PI4P[10]. We found that GTP hydrolysis was enhanced by 2.4-fold in the presence of PI4P (Fig. 2c), suggesting that PI4P improves G protein coupling and GTPase activity. PI and PIP2 also enhanced 5-HT_{1A}-mediated GTP hydrolysis but to a lesser extent (Fig. 2c). Phosphatidylethanolamine (PE) and phosphatidylcholine (PC), which are the major membrane phospholipids, as well as phosphatidylglycerol (PG) and phosphatidylserine (PS), also had modest effects on GTPase activity but significantly lower than PI4P, demonstrating the specific role of PI4P in enhancing 5-HT_{1A} activity (Fig. 2c). On the other hand, PI4P elevated the 5-HT_{1A} basal activity and increased the efficacy of 5-HT_{1A}-mediated recruitment of G_i-protein, suggesting that PI4P can act as a positive allosteric modulator of 5-HT_{1A} (Fig. 2d). Mutations on the PI4P binding residues $R134^{3x50}A$, $K345^{6x35}A$, $K405^{8x48}A$ of 5-HT_{1A} reduced the G-protein activation and abolished the regulatory function of PI4P (Fig. 2e).

In addition to the bound PI4P, 5-HT_{1A} is surrounded by an extensive set of lipid molecules at the membrane interface, including 10 cholesterol molecules and three acyl tails from phospholipids (Fig. 2f). These lipid molecules are well defined in the EM density maps (Fig. 2f, Extended Data Fig. 3a-c). Interestingly, one of the two acyl chains of PI4P is sandwiched between two cholesterol molecules, suggesting that cholesterols play a role in stabilizing PI4P binding (Fig. 2f, Extended Data Fig. 4a-c). These observations illustrate that cholesterol directly participates in the binding of PI4P (CHL #2 and #3 in Fig. 2f, Extended Data Fig. 4a-c), therefore providing a structural basis for the long-standing observation that 5-HT_{1A} signaling is modulated by cholesterol and phospholipids[23,24].

Ligand activation of 5-HT receptors

Our agonist- and G protein-bound structures are in the active state. Compared to the inactive 5-HT_{1B} structure[20], the active 5-HT_{1A}, 5-HT_{1D}, and 5-HT_{1e} structures undergo a common set of structural rearrangements[21,25], including agonist-induced outward movement at the cytoplasmic end of TM6. As illustrated by the 5-HT_{1A} complexes, the binding of 5-HT or aripiprazole within the orthosteric pocket presses a downward swing of the toggle switch W^{6x48} (Extended Data Fig. 5c), which leads to conformational changes of F^{6x44} and I^{3x40} in the PIF motif (Extended Data Fig. 5d) and R^{3x50} in the DRY motif. These conformational changes lead to the breakage of the conserved ionic lock between TM3 and TM6, leading to a large outward movement of TM6 by as much as 9 Å at the Cα of E^{6x30} at the cytoplasmic end of TM6. In addition, the cytoplasmic end of TM7 has an inward movement of ~5.0 Å, which allows Y^{7x53} from the NPxxY motif, together with Y^{5x58}, to form hydrogen bonds with R^{3x50} of the DRY motif. These conformational changes open the receptor cytoplasmic pocket for Gi binding.

Basis for basal activation of 5-HT_{1A}

We could generate a stable 5-HT_{1A}-G_i complex in the apo state, consistent with the high basal activity of 5-HT_{1A}, which was inhibited by methiothepin, an inverse agonist[20] and to a less extent, by WAY-100635, a neutral antagonist[26] (Extended Data Fig. 5a). The overall structure of the apo-complex is highly similar to the 5-HT bound complex (Extended Data Fig. 1). The EM map clearly reveals several structured water molecules that form hydrogen bonds with the receptor within the orthosteric binding pocket (Fig. 3a, b, Extended Data Fig. 5b), where the local resolution is in the range of 2.5-2.8 Å (Extended Data Fig. 1h). These water molecules are arranged in the same spatial plane as 5-HT (Fig. 3b). Three water molecules overlap with the positions of the serotonin hydroxyl (W1), indole nitrogen (W2), and primary amine (W3) functionalities, respectively (Fig. 3b). The latter water molecule (W3) forms a hydrogen bond with D116^{3x32}, which is conserved in aminergic GPCRs where it binds the canonical primary amine of endogenous ligands (Fig. 3b). W2 is proximal to the toggle residue W358^{6x48}, which is an important determinant of GPCR activation[27] (Extended Data Fig. 5e). The presence of water molecules resembles all three polar functionalities of serotonin in the active apo-5-HT_{1A}-G_i complex, thus contributing to the stabilization of 5-HT_{1A} in the active conformation.

To investigate the role of water molecules in the binding pocket, we performed additional MD simulations involving the active apo 5-HT_{1A} receptor and the inactive apo 5-HT_{1A} receptor. Two 100-ns simulations were produced for each system. In the active apo receptor simulations, the functionally important residues D116^{3x32}, S199^{5x43} and T121^{3x37} could be stabilized by the hydrogen-bonding network of five water molecules (Extend data Figure. 5g, h). Such hydrogen-bonding network was maintained in 68.8% simulation trajectories of the active apo receptor system. However, in the inactive apo receptor system, the TM6 helix is positioned away from TM5 at the extracellular side, which yields to a larger pocket and accommodates more water molecules (Extend data Figure. 5i). Consequentially, the hydrogen-bonding network linking D116^{3x32}, T121^{3x37} and S199^{5x43} seen in the active apo receptor system was only observed in 14.1% simulation trajectories of the inactive apo receptor system.

Basis for 5-HT pan agonism

To determine the basis of pan-agonism of 5-HT, we performed pairwise comparisons of the 5-HT_{1A}, 5-HT_{1D}, and 5-HT_{1e} structures. 5-HT has very similar affinities for 5-HT_{1A} and 5-HT_{1D} (pK_i of 8.4 and 8.5, respectively)[28]. A comparison with the binding mode of 5-HT in the 5-HT_{1A} and the 5-HT_{1D} structure reveals a nearly overlapped conformation of 5-HT be adopted in both 5-HT_{1A} and 5-HT_{1D} (Fig. 3c, Extended Data Fig. 6a-f), which were further supported by mutagenesis (Extended Data Fig. 7, Supplementary Fig.2). Residues that make up the 5-HT binding pockets have a moderate-to-high sequence conservation (73% identity and 95% similarity) among 5-HT receptors. Only eight out of 22 ligand pocket residues (within 5 Å around of serotonin) are identical among all 12 serotonin GPCRs (Extended Data Fig.8), whereas the other 14 residues can vary from receptor to receptor. Together, this shows that all parts of 5-HT can form varying interactions within the 12 serotonin GPCR

subtypes, providing evidence of how GPCRs can interact with the same endogenous ligand with similar affinities and functional responses, a basis for the pan agonism of serotonin.

Drug recognition of 5-HT receptors

Selective and non-selective ligands of 5-HT receptors have been developed into treatments for many neuronal diseases and the five structures reported in this paper have provided a solid foundation to understand ligand selectivity and drug recognition by serotonin receptors. Specifically, BRL-54443 is a selective agonist for 5-HT_{1e} and 5-HT_{1F} with affinities 10- to 100-fold higher than for other 5-HT receptors and dopamine receptors[29]. G protein recruitment assays showed that BRL-54443 is a full agonist for 5-HT_{1e} with an EC_{50} of ~7 nM, but has 15-fold and 100-fold weaker potency for 5-HT_{1D} and 5-HT_{1A}, respectively (Fig. 3h, Extended Data Fig.7, Supplementary Fig.2). BRL-54443 in 5-HT_{1e} occupies the same orthosteric pocket as 5-HT in 5-HT_{1A} and 5-HT_{1D} (Fig. 3d). However, $E311^{6x55}$ in the 5-HT_{1e} pocket forms an extra hydrogen bond with the hydroxyl group of BRL-54443, while the corresponding interaction is missing for the homologous positions $S321^{6x55}$ in 5-HT_{1D} and $A365^{6x55}$ in 5-HT_{1A} (Fig. 3d, Extended Data Fig. 6). Mutations of $E311^{6x55}$ in 5-HT_{1e} to the corresponding residues in 5-HT_{1D} and 5-HT_{1A} reduced BRL-54443 induced 5-HT_{1e} activation by 9-fold and 13-fold, respectively (Extended Data Fig. 7, Supplementary Fig.2). Conversely, 5-HT_{1A} with an $A365^{6x55}$E mutation enhanced the potency of BRL-54443 (Supplementary Fig.2a). These results indicate that the residue at position 6x55 is a key determinant for BRL-54443 selectivity of 5-HT receptors. Furthermore, mutations on K^{6x54}, which interacts with E^{6x55} but not directly with BRL-54443, reduced the 5-HT_{1e} mediated G_i recruitment efficacy by BRL-54443 (Supplementary Fig.2c). Mutation of E^{6x55} and K^{6x54} of 5-HT_{1e} to the corresponding residues of 5-HT_{1A} (A^{6x55} and V^{6x54}) abolished the G_i recruitment efficacy (Supplementary Fig.2c). These results suggest the K^{6x54} stabilize the conformation of residue E^{6x55} allowing it to form a H-bond with BRL-54443 with a favored distance. Throughout the 5-HT receptor subfamily, only 5-HT_{1F} share the same residues of E^{6x55} and K^{6x54} as 5-HT_{1e}, consistent with the selectivity of BRL54443 to 5-HT_{1e} and 5-HT_{1F} over other 5-HT receptors.

In contrast to BRL-54443, 5-carboxamidotryptamine (5-CT), which is a 5-HT mimic with the replacement of the 5-hydroxyl by a bulkier carboxamide, exhibits high affinity (~1 nM) for 5-HT_{1A}, 5-HT_{1B}, and 5-HT_{1D} receptors, which possess smaller Ala and Ser residues in position 6x55, but only modest to weak affinity (~1 μM) for 5-HT_{1e} and 5-HT_{1F} (Extended Data Fig. 8b, 9c). Replacement of $E311^{6x55}$ for Ser or Ala in 5-HT_{1e} increased the potency of 5-CT by 100 to 400 folds (Extended Data Fig. 9e), supporting that residue 6x55 is the determinant for this observed subtype selectivity[30]. To confirm this hypothesis, we correlated the residue types at 6x55 with the binding affinities of 5-HT, 5-MeOT, 5-CT, and Donitriptan (Extended Data Fig.8b). A regression of the affinity versus residue type as a qualitative variable gave R^2 values of 0.97, 0.79, and 0.71 for Donitriptan, 5-CT, and 5-MeOT, respectively (Extended Data Fig. 9a). A considerably weaker correlation was obtained for 5-HT (R^2 = 0.43), reflecting the promiscuity of 5-HT as a pan agonist of serotonin receptors.

Structural analyses of $5HT_{1A,}$ $5\text{-}HT_{1D,}$ $5\text{-}HT_{1e}$ also revealed the basis for the recognition of aripiprazole, one of the best-selling antipsychotic drugs. Aripiprazole displays differential affinities to various members of the $5\text{-}HT_1$ subfamily, with a 5 nM affinity for $5\text{-}HT_{1A}$ but with 10-1000 fold weaker affinities for $5\text{-}HT_{1B}$, $5\text{-}HT_{1D}$, and $5\text{-}HT_{1e}$ [31]. The extracellular end of TM7, which directly participates in the formation of the extended ligand binding pocket, is shifted outward by approximately 3 Å in $5\text{-}HT_{1A}$ relative to the TM7 position in $5\text{-}HT_{1B}$, $5\text{-}HT_{1D}$, and $5\text{-}HT_{1e}$ (Fig. 4). Together with $F112^{3x28}$ and $Y96^{2x63}$, TM7 stabilizes the quinolinone group of aripiprazole in $5\text{-}HT_{1A}$ (Fig. 4). For $5\text{-}HT_{1B}$, $5\text{-}HT_{1D}$, and $5\text{-}HT_{1e}$, the inward movement of the extracellular end of TM7 and the larger side chain of W^{3x28} (corresponding to $F122^{3x28}$ at $5HT_{1A}$) would overlap with the same binding space of the quinolinone group, resulting in a lower affinity of aripiprazole to these receptors (Fig. 4). Notably, one of the most visible cholesterols is inserted into a cleft between TM1 and TM7 and serves as a structural chaperone for these two helices (Fig. 2f, Fig. 4). This cholesterol is involved in the shaping of the ligand pocket and stabilizes the positions of TM1 and TM7 near the quinolinone group, resulting in the higher affinity of aripiprazole for $5\text{-}HT_{1A}$. This is consistent with the important roles of cholesterol in the functional regulation of $5\text{-}HT_{1A}$ [32]. No cholesterol has been observed at the corresponding site in the structures of $5\text{-}HT_{1B}$ [21], $5\text{-}HT_{1D}$, and $5\text{-}HT_{1e}$ (Fig. 1). In addition, cholesterols are also directly involved in the binding of PI4P to enhance G protein coupling and signaling activity (Extended Data Fig. 4).

In summary, we have determined five structures of three different serotonin receptors. These structures reveal an unexpected role of phospholipid PI4P and cholesterol in G protein coupling and ligand recognition. The structures also reveal the basis of basal activation and 5-HT pan agonism as well as the basis for drug recognition at serotonin receptors. These observations have a wide implication in mechanistic understanding of serotonin signaling and drug discovery targeting this important family of receptors.

Methods

Constructs

The human $5\text{-}HT_{1A}$, $5\text{-}HT_{1D}$, and $5\text{-}HT_{1e}$ were modified to contain the N-terminal thermally stabilized BRIL[33] to enhance receptor expression and the addition of affinity tags including N-terminal Flag tag and His tag. $L125^{3x41}W$, $L127^{3x41}W$, and $L111^{3x41}W$ mutations were separately introduced to $5\text{-}HT_{1A}$, $5\text{-}HT_{1D}$, and $5\text{-}HT_{1e}$ to improve thermal stability[34,35]. The N-terminal 24-residue truncated $5\text{-}HT_{1A}$ and the full-length receptors of $5\text{-}HT_{1D}$ and $5\text{-}HT_{1e}$ were cloned into the pFastBac (Thermo Fisher) vector using ClonExpress II One Step Cloning Kit (Vazyme Biotech Co.,Ltd). A dominant-negative human $G\alpha_{i1}$ was generated by site-directed mutagenesis to incorporate mutations S47N, G203A, A326S, and E245A that improves the dominant-negative effect by weakening a salt bridge that helps to stabilize the interactions with the $\beta\gamma$ subunits[19]. Human $DNG\alpha_{i1}$, human $WTG\alpha_{i1}$, human $G\beta_1$, human $G\gamma_2$ and a single chain antibody scFv16[36] were cloned into pFastBac vectors. These constructs were generated in insect cell expression vectors.

Insect cell expression

Human 5-HT_{1A}, 5-HT_{1D}, and 5-HT_{1e}, human DNGα_{i1}, human Gβ_1, and human Gγ_2 were co-expressed in Spodoptera frugiperda Sf9 insect cells (Invitrogen) using the baculovirus method (Expression Systems). For the 5-HT_{1D}–G_i and 5-HT_{1e}–G_i complexes, scFv16 was co-expressed to stabilize the protein. As for the apo–5-HT_{1A}–G_i (WT) complex used for GTPase assay, the DNGα_{i1} was replaced by WTGα_{i1}. Cell cultures were grown in ESF 921 serum-free medium (Expression Systems) to a density of 2-3 million cells per ml and then infected with four separate baculoviruses at a suitable ratio. The culture was collected by centrifugation 48 h after infection and cell pellets were stored at -80°C.

Complex purification

Cell pellets were thawed in 20 mM HEPES pH 7.4, 50 mM NaCl, 10 mM $MgCl_2$ supplemented with Protease Inhibitor Cocktail (Bimake). For the apo–5-HT_{1A}–G_i complex, 25 mU/ml apyrase (Sigma) was added; for the 5-HT- or aripiprazole-bound 5-HT_{1A}–G_i complexes, 20 μM 5-HT (TargetMol) or aripiprazole (TargetMol) and 25 mU/ml apyrase (Sigma) were added; for the 5-HT_{1D}–G_i–scFv16 complex, 20 μM 5-HT (TargetMol) and 25 mU/ml apyrase (Sigma) were added; for the 5-HT_{1e}–G_i–scFv16 complex, 20 μM BRL-54443 (TargetMol) and 25 mU/ml apyrase (Sigma) were added. The suspension was incubated for 1 h at room temperature and the complex was solubilized from the membrane using 0.5% (w/v) n-dodecyl-β-d-maltoside (DDM, Anatrace) and 0.1% (w/v) cholesteryl hemisuccinate (CHS, Anatrace) for 2 h at 4°C. Insoluble material was removed by centrifugation at 65,000 g for 30 min and the solubilized complex was immobilized by batch binding to Talon affinity resin. After that, the resin was packed and washed with 20 column volumes of 20 mM HEPES pH 7.4, 100 mM NaCl, 5 mM $MgCl_2$, 0.01% (w/v) lauryl maltose neopentylglycol (LMNG, Anatrace), and 0.002% (w/v) CHS. The complex was then eluted in buffer containing 300 mM imidazole and concentrated using an Amicon Ultra Centrifugal Filter (MWCO 100 kDa). The complex was subjected to size-exclusion chromatography on a Superdex 200 Increase 10/300 column (GE Healthcare) pre-equilibrated with Size Buffer containing 20 mM HEPES pH 7.4, 100 mM NaCl, 0.00075% (w/v) LMNG, 0.00025% (w/v) GDN (Anatrace), and 0.00015% CHS to separate complex from contaminants. For the ligand-bound complexes, 20 μM corresponding ligand was contained in the Size Buffer. Eluted fractions were evaluated by SDS-PAGE (Supplementary Fig.1) and consisting of receptor–G_i-protein complex were pooled and concentrated for EM experiments.

Peptidisc reconstitution and GTPase assay

Peptide NSPr (FAEKFKEAVKDYFAKFWDPAAEKLKEAVKDYFAKLWD) was used for peptidisc reconstitutions with different lipid compositions. The reconstitution was based on methods previously reports[22,37]. In brief, the purified 5-HT_{1A}–G_i (WT) complex was mixed with NSPr, lipids, LMNG, and cholesterol at optimized ratios. Reconstitution mixture was incubated overnight at 4℃. Then the samples were subjected to Bio-Beads SM2 (50 mg/ml; Bio-Rad) twice for total 8 h at 4℃ to remove detergent. The mixture was spun down, and the supernatant was loaded on to TALON beads to remove empty peptidiscs. After binding for 3 h at 4℃, the beads were washed with 20 mM HEPES pH 7.4, 100 mM NaCl and the lipid-

containing 5-HT_{1A}–G_i peptidiscs were eluted with 20 mM HEPES pH 7.4, 100 mM NaCl, 250 mM Imidazole. The samples were applied onto a Superdex 200 Increase 10/300 column (GE Healthcare) pre-equilibrated with 20 mM HEPES pH 7.4, 100 mM NaCl. The peak corresponding to the 5-HT_{1A}–G_i peptidiscs was collected for the GTPase-Glo assay. A modified protocol of the GTPase-Glo™ Assay (Promega) was used to detect the GTPase activity of the G-protein[10]. In this assay, the amount of GTP depends on the degree of hydrolysis by G-protein or activated receptor-bound G-protein. The remaining GTP be converted to ATP by GTPase-Glo reagent, then converted to luminescent signal by detection reagent. To analyses the regulating effect of lipids, the GTPase reaction with 5-HT_{1A}–G_i peptidisc started in an assay buffer containing 20 mM HEPES, pH 7.4, 100 mM NaCl, 1 mM DTT, 5 μM GDP and 5 μM GTP. After 60 min incubation, the detection reagent was added and then incubated for 30 min at room temperature. Luminescence was measured using EnVison® (PerkinElmer).

NanoBiT G-protein recruitment assay

Analysis of G_i-protein recruitment was performed by using a modified protocol of the NanoBiT system (Promega) described previously[30]. NanoBiT system is a two-subunit system based on NanoLuc luciferase that can be used for functional detection for binding and dissociation of GPCR and G-protein. LgBiT (17.6 kDa) of the NanoBiT luciferase was fused to the C-terminal of GPCR with 15-amino acid flexible linkers. SmBiT was C-terminally fused to Gβ subunit with a 15-amino acid flexible linker. Human 5-HT_{1A}-LgBiT, 5-HT_{1D}-LgBiT, and 5-HT_{1e}-LgBiT, WTGα_{i1}, SmBiT-fused Gβ_1, and Gγ_2 were co-expressed in Spodoptera frugiperda Sf9 insect cells using the baculovirus method (Expression Systems). Cell cultures were grown to a density of 2-3 million cells per ml and then infected with four separate baculoviruses at a suitable ratio. The culture was collected by centrifugation 48 h after infection and cell pellets were collected with PBS. The cell suspension was dispensed in a white 384-well plate at a volume of 40 μl per well and loaded with 5 μl of 90 μM coelenterazine (Yeasen) diluted in the assay buffer. Test compounds (5 μl) were added and incubated for 3-5 min at room temperature before measurement. Luminescence counts were normalized to the initial count and fold-change signals over vehicle treatment were used to show G-protein binding response.

Cryo-EM grid preparation and data acquisition

Three microliters of the purified agonist-bound 5-HT_{1A}, 5-HT_{1D}, and 5-HT_{1e} complexes at ~5 mg/ml, 30 mg/ml, 45 mg/ml, respectively, were applied onto a glow-discharged Quantifoil R1.2/1.3 200-mesh gold holey carbon grid. The grids were blotted for 3 s under 100% humidity at 4 °C and then vitrified by plunging into liquid ethane using a Vitrobot Mark IV (Thermo Fischer Scientific). For the 5-HT_{1A} complexes, cryo-EM data collection was performed on a Titan Krios at 300 kV accelerating voltage in the Center of Cryo-Electron Microscopy, Zhejiang University (Hangzhou, China) and the micrographs were recorded using a K2 Summit direct electron detector (Gatan) in counting mode at a calibrated magnification of 1.014 Å per pixel. Micrographs were obtained at a dose rate of about 8.0 e/$Å^2$/s with a defocus ranging from -1.0 to -3.0 μm. Each micrograph was dose-fractionated to 40 frames with a total exposure time of 8 s. For the 5-HT_{1D} and 5-HT_{1e} complexes, cryo-EM data collection was performed on a Titan Krios at 300 kV accelerating

voltage in the Center of Cryo-Electron Microscopy, Shanghai Institute of Materia Medica, Chinese Academy of Sciences (Shanghai, China). The micrographs were recorded using a K3 Summit direct electron detector (Gatan) with a Gatan energy filter (operated with a slit width of 20 eV) (GIF). The microscope was operated at a magnification of 47,847 in counting mode, corresponding to pixel size of micrograph at 1.045 Å. The images were recorded at a dose rate of about 26.7 e/Å^2/s with a defocus ranging from -1.0 to -3.0 μm. The total exposure time was 3 s and intermediate frames were recorded in 0.083 s intervals, resulting in a total of 36 frames per micrograph. A total of 4179, 5269, 2005, 4375, and 5249 movies were collected for the apo-, 5-HT bound-, aripiprazole bound- 5-HT$_{1A}$–G$_i$, 5-HT bound- 5-HT$_{1D}$–G$_i$, and BRL-54443 bound- 5-HT$_{1e}$–G$_i$ complexes, respectively.

Image processing and 3D reconstruction

Image stacks were subjected to beam-induced motion correction using MotionCor2.1[38]. Contrast transfer function (CTF) parameters for each non-dose weighted micrograph were determined by Gctf[39]. Automated particle selection and data processing were performed using Relion-3.0-beta2[40]. For the dataset of 5-HT bound 5-HT$_{1A}$–G$_i$ complex, automated particle selection yielded 5,279,538 particles. The particles were extracted on a binned dataset with a pixel size of 2.028 Å and were subjected to reference-free 2D classification, producing 898,450 particles with well-defined averages. The map of NTSR1–G$_{i1}$ complex (EMDB-20180)[41] low-pass filtered to 40 Å was used as an initial reference model for 3D classification, which produces two good subsets showing clear structural features accounting for 559,323 particles. Further 3D classifications focusing the alignment on the complex except AHD of the Gα, produced three high-quality subsets accounting for 472,338 particles. These particles were subsequently subjected to Bayesian polishing, CTF refinement and 3D refinement, which generated a map with an indicated global resolution of 3.0 Å at a Fourier shell correlation of 0.143. For the dataset of apo–5-HT$_{1A}$–G$_i$ complex, particle selection yielded 2,719,825 particles, which were subjected to reference-free 2D classification, producing 1,922,844 particles for further processing. The map of 5-HT–5-HT$_{1A}$–G$_i$ complex low-pass filtered to 20 Å was used as an initial reference model for 3D classification, which produces one good subset accounting for 680,449 particles. Further 2 rounds of 3D classifications focusing the alignment on the complex except AHD of the Gα, produced the high-quality subsets accounting for 245,886 particles. These particles were subsequently subjected to Bayesian polishing, CTF refinement and 3D refinement, which generated a map with an indicated global resolution of 3.0 Å at a Fourier shell correlation of 0.143. For the dataset of aripiprazole–5-HT$_{1A}$–G$_i$ complex, a total of 1,486,169 particles were automatically picked and extracted on a binned 2 dataset. These particles were subjected to reference-free 2D classification, producing 748,746 particles with well-defined averages for further processing. The map of apo–5-HT$_{1A}$–G$_i$ complex low-pass filtered to 20 Å was used as an initial reference model for 3D classification, which produces one good subset. Further 3D classifications focusing the alignment on the complex, produced one high-quality subset accounting for 154,241 particles. These particles were subsequently subjected to 3D refinement and Bayesian polishing, which generated a map with an indicated global resolution of 3.1 Å according to the 0.143 criteria of the FSC. For the dataset of 5-HT–5-HT$_{1D}$–G$_i$ complex, particle selection yielded 4,212,737 particles. The particles were subjected to reference-free 2D classification, producing 2,361,598 particles

with good features. The map of 5-HT–5-HT_{1A}–G_i complex low-pass filtered to 60 Å was used as an initial model for 3D classification, which produces one good subset accounting for 896,076 particles. Further 3D classifications focusing the alignment on the receptor and the receptor–G_i complex, produced one high-quality subset accounting for 141,501 particles. These particles were subsequently subjected to CTF refinement and Bayesian polishing, which generated a map with an indicated global resolution of 2.9 Å. For the dataset of BRL54443–5-HT_{1e}–G_i complex, automated particle selection yielded 4,977,538 particles, which were subjected to 2D classification. 2,175,234 particles with well-defined averages were selected for further 3D classification processing. The map of 5-HT–5-HT_{1A}–G_i complex low-pass filtered to 60 Å was used as an initial reference model for 3D classification, which produces one good subset accounting for 1,156,885 particles. Further 3D classifications focusing the alignment on the receptor and the entire complex, produced the two subsets with good receptor density. The two subsets accounting for 163,354 particles were subsequently subjected to CTF refinement, Bayesian polishing and 3D refinement, which produced a map with an indicated global resolution of 2.9 Å according to 0.143 criterion of the FSC. Local resolution was determined using the Bsoft package[42] with half maps as input maps.

Structure determination and refinement

The cryo-EM structures of the apo–5-HT_{1A}–G_i, 5-HT–5-HT_{1A}–G_i, aripiprazole–5-HT_{1A}–G_i, 5-HT–5-HT_{1D}–G_i–scFv16, and BRL-54443–5-HT_{1e}–G_i–scFv16 complexes were solved using 5-HT_{1B} (PDB code: 6G79)[21] and rhodopsin–G_i complex (PDB code: 6CMO)[43] as initial models. The models were docked into the electron microscopy density maps using Chimera[44], followed by iterative manual adjustment and rebuilding in COOT[45] and ISOLDE[46], against the cryo-EM electron density maps. Real space and reciprocal refinements were performed using Phenix[47]. The model statistics was validated using MolProbity[48]. Structural figures were prepared in Chimera[44], ChimeraX[49] and PyMOL (https://pymol.org/2/). The final refinement statistics are provided in Extended Data Table 1.

Molecular docking

The structures of 5-HT_{1A}, 5-HT_{1B} (PDB code: 6G79), 5-HT_{1D}, and 5-HT_{1e} were employed to build the molecular docking models. All ligands and water molecules in these structures were removed to generate the models. The structures of the small-molecule ligands of interest were download from the PubChem database (www. pubchem.ncbi.nlm.nih.gov). A ligand was docked to the proposed ligand-binding pocket of its receptor using Schrodinger Glide software in SP mode with default parameters[50]. The ligand was initially placed in the center of the pocket and was constrained to move within a 1 nm diameter sphere, where it was allowed to move freely during the docking process. The extended conformation searches were performed using the Lamarckian Genetic Algorithm. Docked poses with most negative docking scores were selected for analysis.

Regression models for ligand affinity

Partial least squares regression models were made for the binding affinity of 5-HT, 5-CT, 5MeOT, and Donitriptan to the 5-HT receptors (Extended Data Figure 8a) and the amino acid residue at position 6x55 as a qualitative variable. Separate models were made for each

ligand and the applied number of principal components was determined by cross-validation. The calculations were made using Simpca-P version 11.0 (https://umetrics.com).

Molecular dynamics simulation.

The active apo 5-HT_{1A} simulation model was built based on the apo–5-HT_{1A}–G_i complex structure. All structured water molecules were included in the simulation system. Using homology modeling method, the inactive 5-HT_{1A} simulation model was built based on the structure of inactive 5-HT_{1B} (PDB code: 5V54) with Modeller[51]. The default parameters were employed to construct the models. The missing backbone and sidechains were added. The models with the lowest root mean square deviations from their template structures were selected. To build a simulation system, we placed the complex model into a 1-palmitoyl-2-oleoyl-sn-glycero-3-phosphocholine lipid bilayer. The lipid embedded complex model was solvated in a periodic boundary condition box (160 Å × 160 Å × 160 Å) filed with TI3P water molecules and 0.15 M KCl using CHARMM-GUI[52]. Each system was replicated to perform two independent simulations. On the basis of the CHARMM all-atom force field[53,54], molecular dynamics simulations were conducted using GROMACS 5.1.4[55,56]. After 100 ns equilibration, a 100 ns production run was carried out for each simulation. All productions were carried out in the NPT ensemble at temperature of 303.15 K and a pressure of 1 atm. Temperature and pressure were controlled using the velocity-rescale thermostat[57] and the Parrinello-Rahman barostat with isotropic coupling[58], respectively. Equations of motion were integrated with a 2 fs time step, the LINCS algorithm was used to constrain bond length[59]. Nonbonded pair lists were generated every 10 steps using distance cutoff of 1.4 nm. A cutoff of 1.2 nm was used for Lennard-Jones (excluding scales 1-4) interactions, which were smoothly switched off between 1 and 1.2 nm. Electrostatic interactions were computed using particle-mesh-Ewald algorithm with a real-space cutoff of 1.2 nm[59].

Europe PMC Funders Author Manuscripts

Extended Data

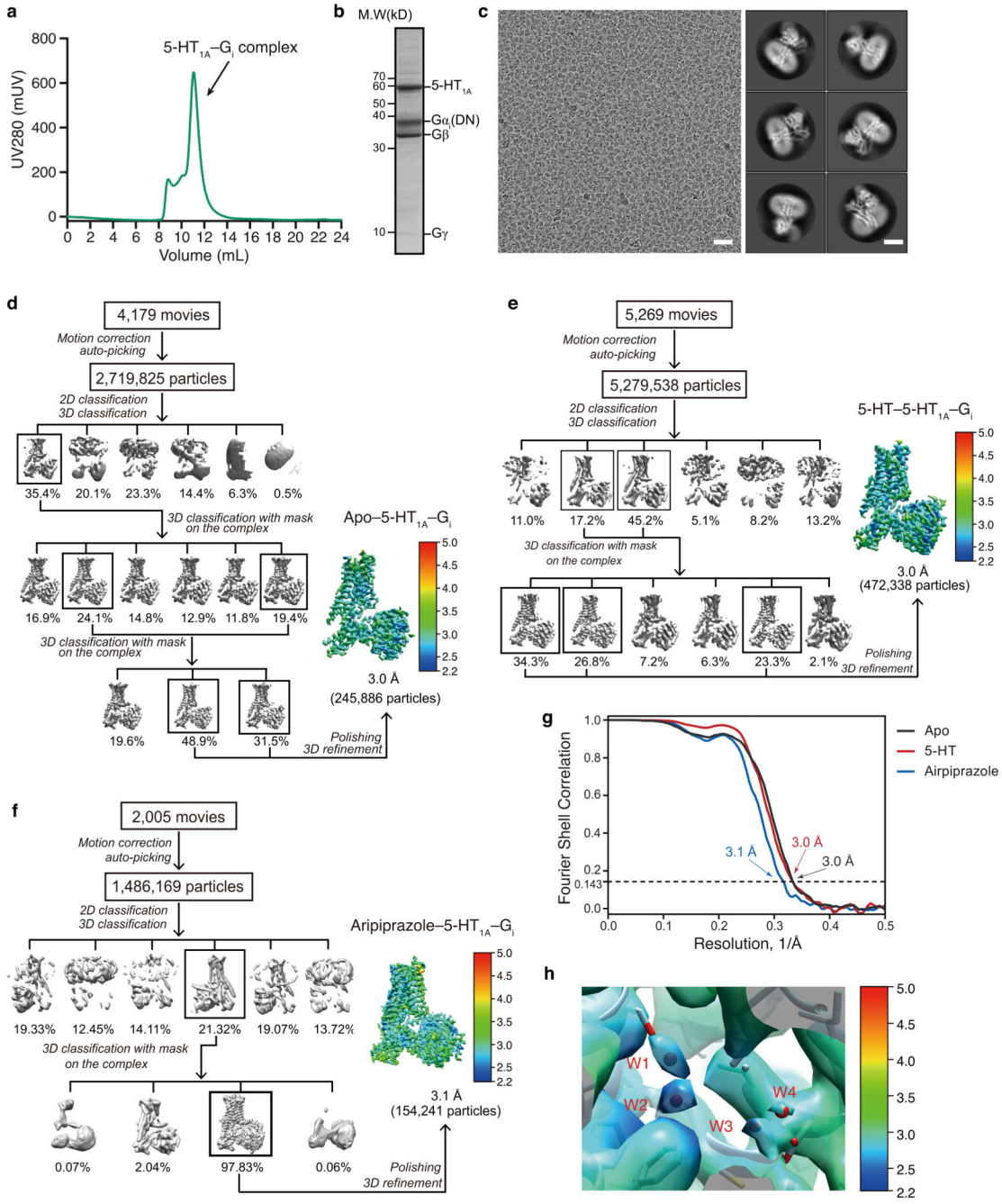

Extended Data Fig. 1. Sample preparation and cryo-EM of the 5-HT$_{1A}$–G$_i$ complexes.

a, Analytical size-exclusion chromatography of the purified complex. **b**, SDS-PAGE/ Coomassie blue stain of the purified complex. Experiments were repeated three times with similar results. **c**, Representative cryo-EM image (scale bar: 30 nm) from 4,179 movies and 2D averages (scale bar: 5 nm) of 5-HT–5-HT$_{1A}$–G$_i$ complex. Experiments were repeated three times with similar results. **d-f**, Flowchart of cryo-EM data analysis and the local

resolution shown for the density of apo- (**d**), serotonin bound- (**e**), and aripiprazole bound- (**f**) 5-HT_{1A}–G_i complexes. **g**, 'Gold-standard' Fourier shell correlation (FSC) curves. **h**, the local resolution shown for the density of water molecules (W1-W4) in the ligand binding pocket of the apo 5-HT_{1A}–G_i structure.

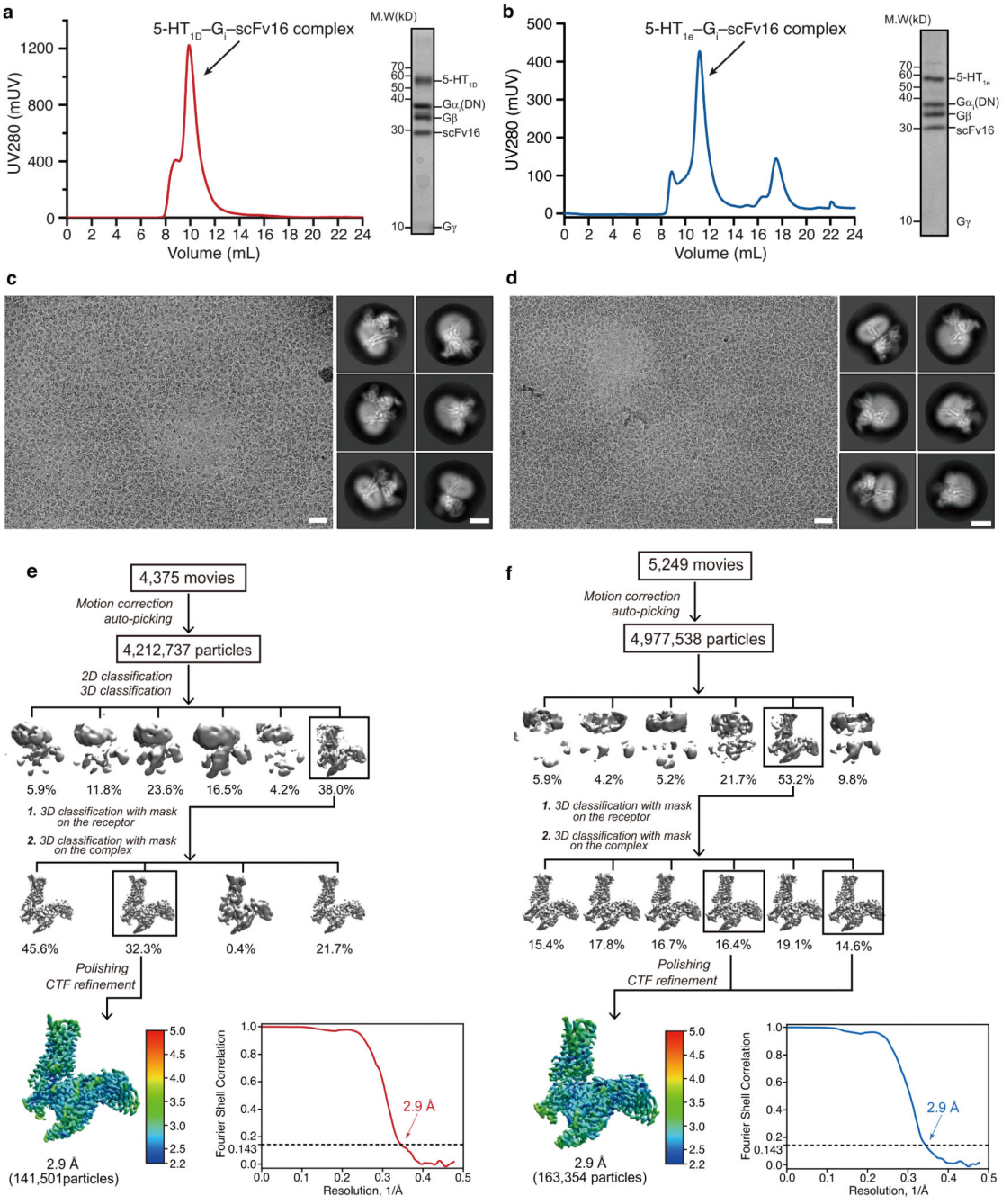

Extended Data Fig. 2. Sample preparation and cryo-EM of the 5-HT_{1D}–G_i–scFv16 and the 5-HT_{1e}–G_i–scFv16 complexes.

a, b, Analytical size-exclusion chromatography and SDS-PAGE/Coomassie blue stain of the purified 5-HT_{1D}–G_i–scFv16 complex (**a**) and the 5-HT_{1e}–G_i–scFv16 complex (**b**).

Europe PMC Funders Author Manuscripts

Experiments were repeated three times with similar results. **c,** Representative cryo-EM image (scale bar: 30 nm) from 4,375 movies and 2D averages (scale bar: 5 nm) of 5-HT_{1D}–G_i–scFv16 complex. **d,** Representative cryo-EM image (scale bar: 30 nm) from 5,249 movies and 2D averages (scale bar: 5 nm) of 5-HT_{1e}–G_i–scFv16 complex. **e, f,** Flowchart of cryo-EM data analysis, the local resolution of the density, and the 'Gold-standard' Fourier shell correlation (FSC) curves of the 5-HT_{1D}–G_i–scFv16 complex (**e**) and the 5-HT_{1e}–G_i–scFv16 complex (**f**).

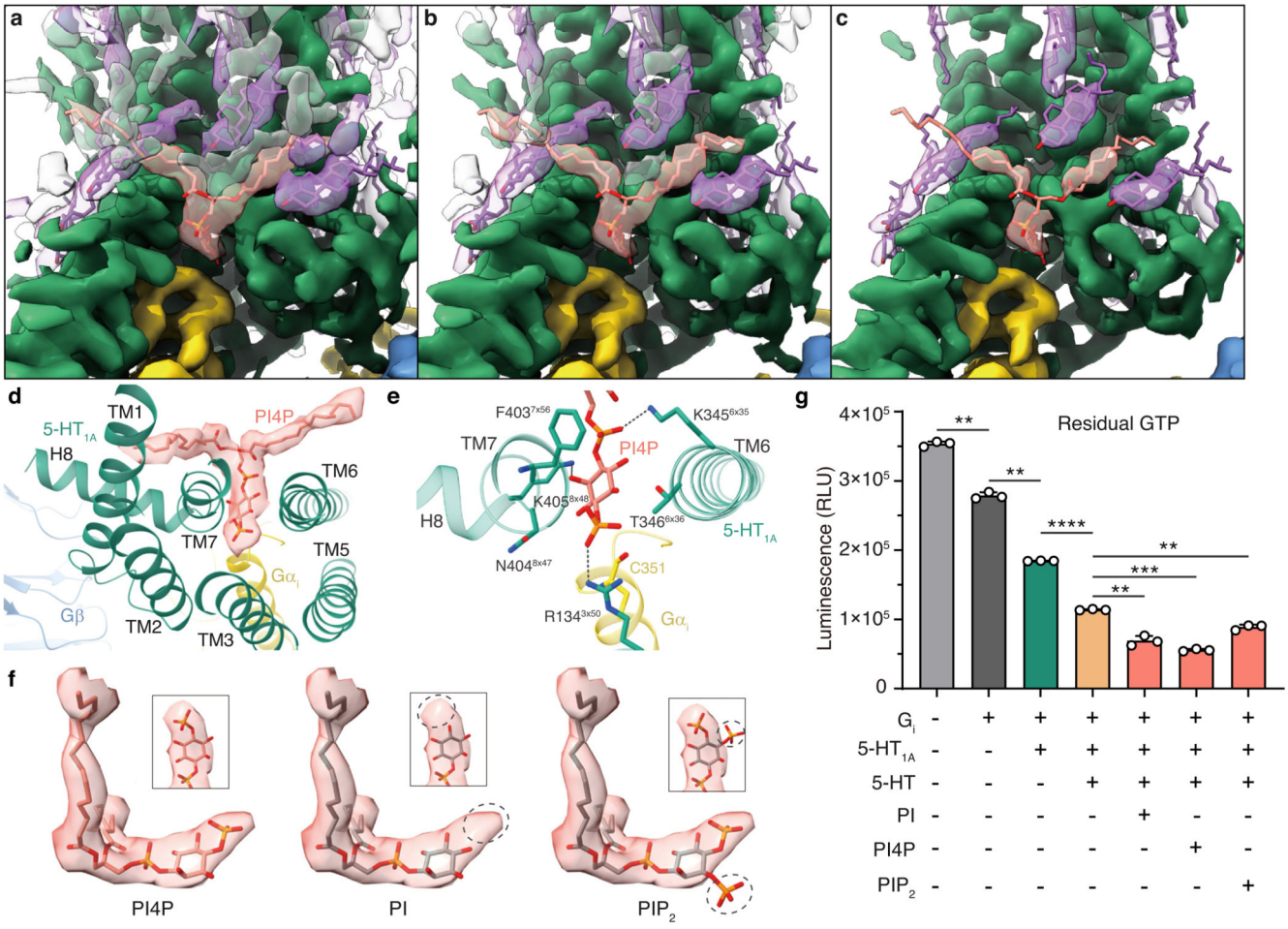

Extended Data Fig. 3. Lipids regulation in 5-HT_{1A} receptor.

a-c, The EM map of apo–5-HT_{1A}–G_i complex and the surrounding lipids are shown with different threshold of 0.025 (**a**), 0.03 (**b**), and 0.04 (**c**). **d**, Interactions of PI4P at the 5-HT_{1A}–G_i interface. **e,** Interaction of the PI4P head group with the TM6/TM7/Gα_i pocket. Hydrogen bonds are shown with dashed lines. **f.** Comparison of the density fitting for PI4P, PI, and PIP2. The place of density that is not fit well is circled by dash line. **g**. 5-HT_{1A}-mediated G_i activity are regulated by PI, PI4P and PIP2 with the greatest degree of PI4P regulation. GTPase-Glo assay was perform in LNMG buffer. Lower levels of residual GTP indicates higher levels of G protein activity upon receptor-mediated GDP/GTP exchange.

Data are presented as mean ± SD of three independent experiments performed in technical triplicate. **p < 0.01; ***p < 0.001; ****p < 0.0001; two-tailed paired t-tests.

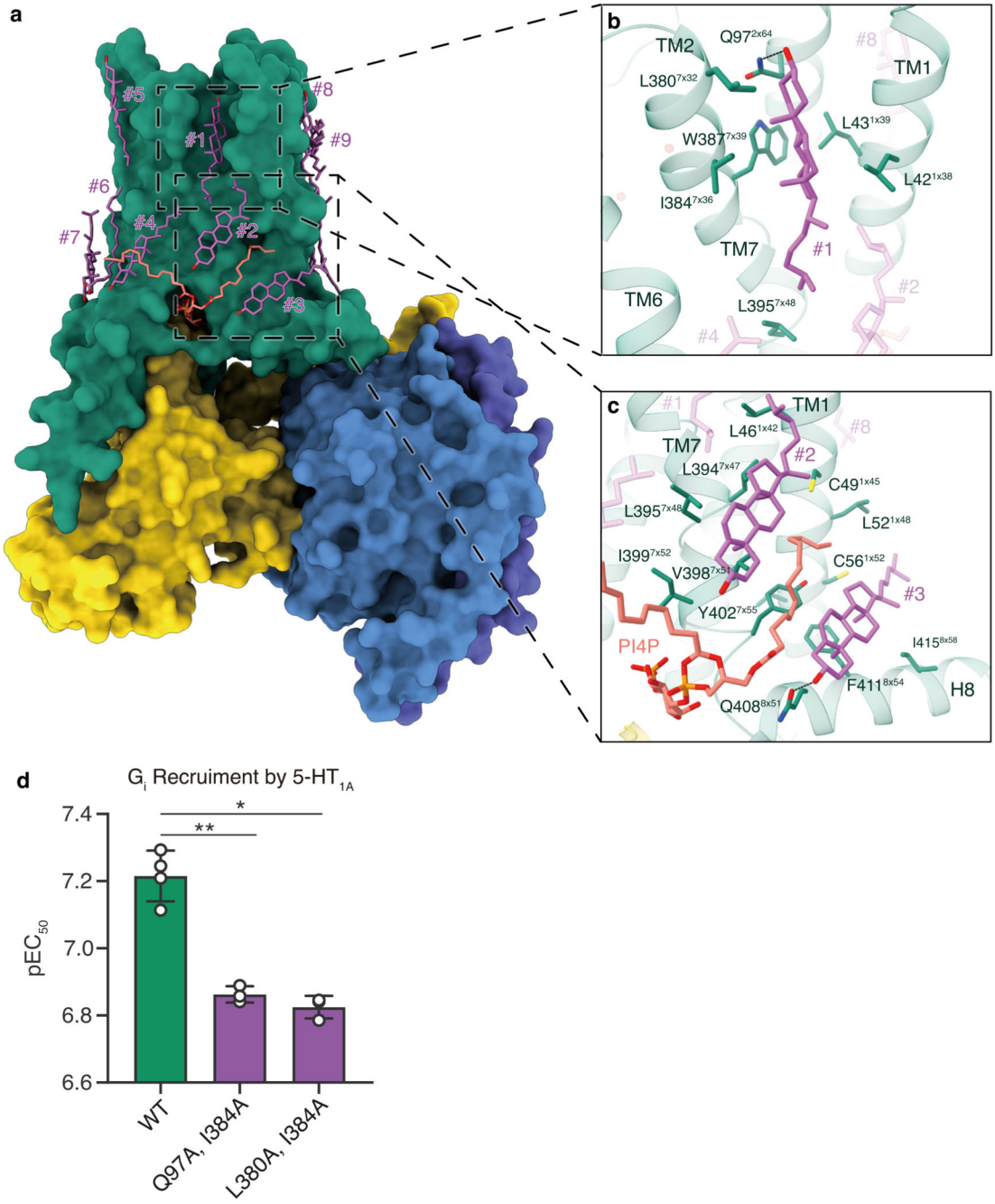

Extended Data Fig. 4. Cholesterol regulation in 5-HT$_{1A}$ receptor.

la, The model of the 5-HT$_{1A}$–G$_i$ complex shows multiple cholesterols bound to the surface of 5-HT$_{1A}$. The 5-HT$_{1A}$–G$_i$ complex is shown as surface and lipids are shown as sticks. **b**, Interactions of CHL #1 with TM1/7 of 5-HT$_{1A}$. **c**, Interactions of CHL #2 and #3 with 5-HT$_{1A}$. **d**. The effect of cholesterol on the 5-HT potency to activate 5-HT$_{1A}$. The effects of

Europe PMC Funders Author Manuscripts

mutations at the binding residues of cholesterol #1 on 5-HT mediated activation of 5-HT_{1A} (pEC50) were detected by NanoBiT recruitment assays. Data are presented as mean ± SD from at least three independent experiments performed in technical triplicate. *p < 0.05; **p < 0.01; two-tailed paired t-tests.

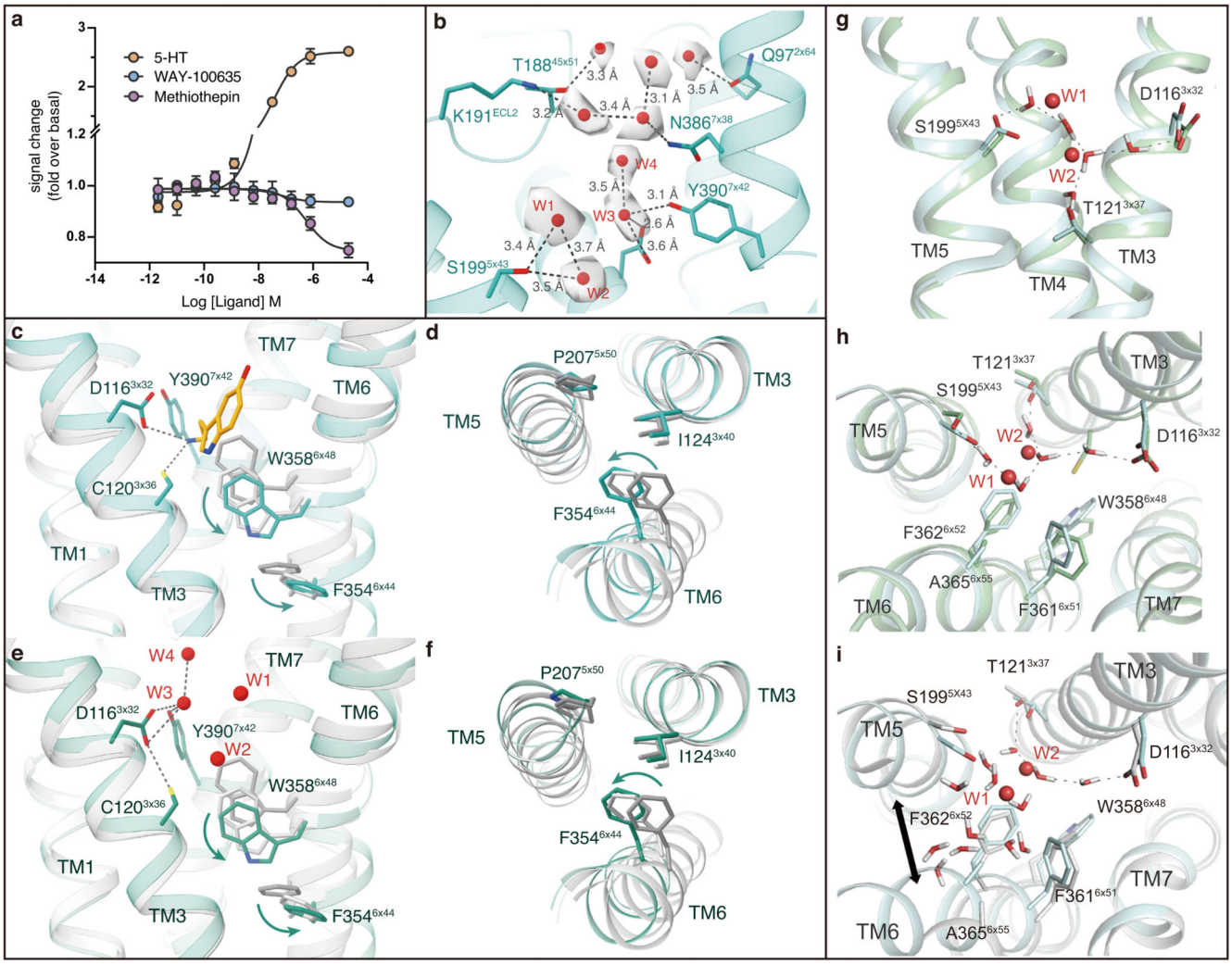

Extended Data Fig. 5. Basal activity and ligand-induced activation of 5-HT_{1A}.

a, Detection of the ligand-reduced activity and constitutive activity of the human 5-HT_{1A} by NanoBiT G-protein recruitment assay. Three ligands, the full agonist 5-HT, the neutral antagonist WAY-100635, and the inverse agonist methiothepin were used. Data are presented as mean ± SEM of three independent experiments performed in technical triplicate. **b**, Water molecules are coordinated in the ligand binding pocket of the apo 5-HT_{1A} structure. The density is shown at 3σ cutoff. **c-f**, Activation of the 5-HT_{1A} by 5-HT and the binding to apo 5-HT_{1A} by water molecules. Toggle switch in 5-HT bound 5-HT_{1A} structure (**c**) and apo 5-HT_{1A} structure (**e**). PIF motif of the 5-HT bound 5-HT_{1A} structure (**d**) and the apo 5-HT_{1A} structure (**f**). The 5-HT bound 5-HT_{1A} structure is colored with turquoise; the apo 5-HT_{1A} is colored with green; 5-HT is colored with orange. Aligned structures of the inactive state 5-

HT_{1B} (inverse agonist methiothepin bound) and the intermediate state 5-HT_{1B} (agonist ERG bound) are colored with gray and light gray. Conformational changes of toggle switch residue $W358^{6.48}$ and the residue $F354^{6.44}$, which is part of a conserved PIF motif, are illustrated by arrows. **g-i**, The hydrogen-bonding network of the ligand-binding pocket observed in the MD simulations. Side view (**g**) and top view (**h**) of a hydrogen-bonding network linking the key residues of the active apo 5-HT_{1A} receptor. **i**, Top view of water molecules accommodated in the inactive apo 5-HT_{1A} receptor. The structure of the apo 5-HT_{1A} is colored in light blue. A representative conformation from the active apo 5-HT_{1A} simulations is colored in light green. A representative conformation from the inactive apo 5-HT_{1A} simulations is colored in gray. The structured water W1 and W2 of the apo 5-HT_{1A}-G_i complex structure are showed as sphere. Putative hydrogen bonds are showed as dash lines.

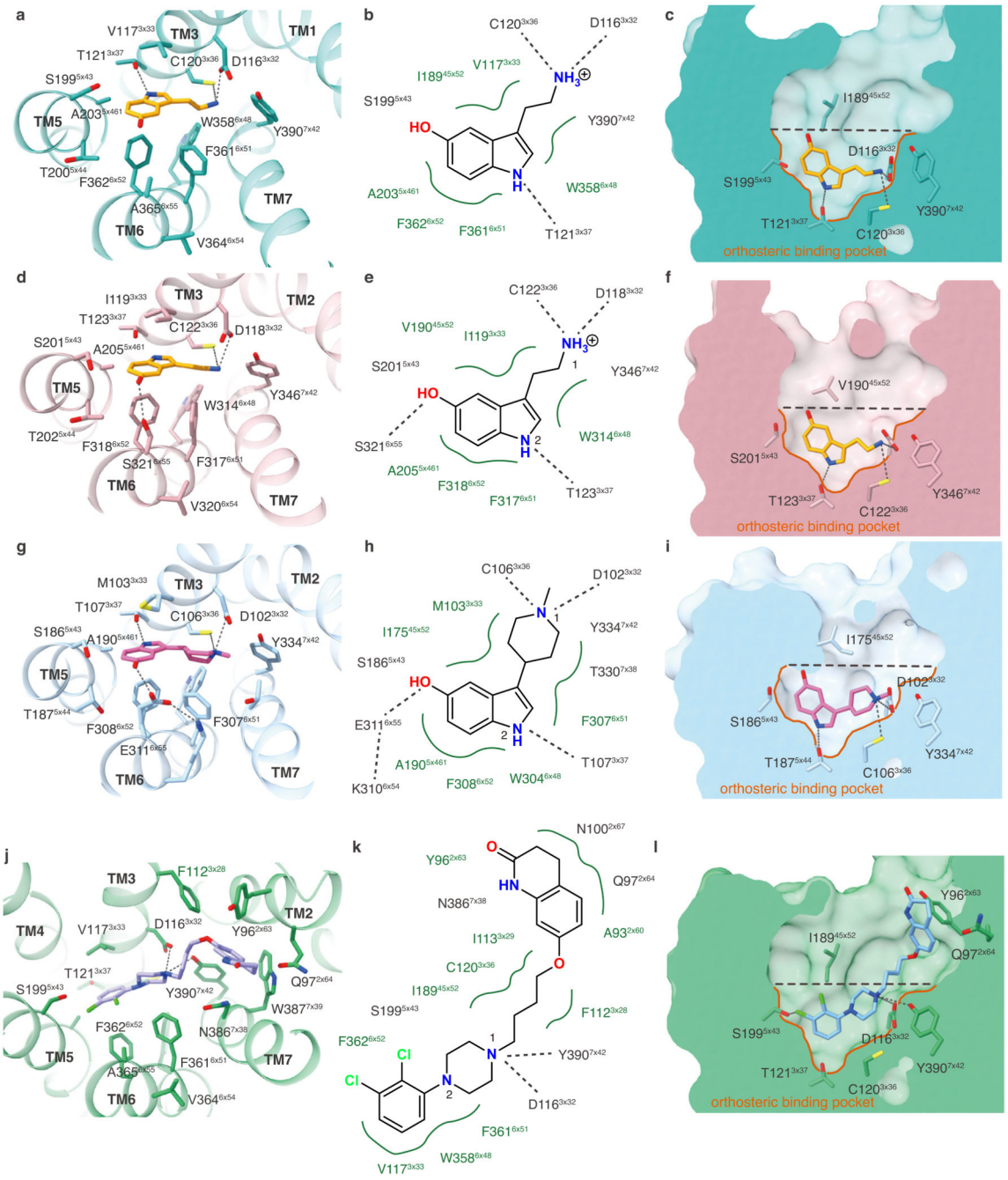

Extended Data Fig. 6. Ligand recognition of the 5-HT$_{1A}$, the 5-HT$_{1D}$ and the 5-HT$_{1e}$.

a, **d**, **g**, **j**, Conformation of the ligand binding pockets in the serotonin bound 5-HT$_{1A}$ (**a**), the serotonin bound 5-HT$_{1D}$ (**d**), the BRL-54443 bound 5-HT$_{1e}$ (**g**), and the aripiprazole bound 5-HT$_{1A}$ (**j**). **b**, **e**, **h**, **k**, Diagram of ligand recognition for serotonin in 5-HT$_{1A}$ (**b**), serotonin in 5-HT$_{1D}$ (**e**), BRL-54443 in 5-HT$_{1e}$ (**h**), and aripiprazole in 5-HT$_{1A}$ (**k**). **c, f, i, l,** Ligand binding pockets shown as surfaces. The orthosteric binding pocket is highlighted in orange.

Europe PMC Funders Author Manuscripts

Pos.	5-HT_{1A} + 5-HT			5-HT_{1D} + 5HT			5-HT_{1e} + BRL54443		
	Mutants	pEC50±SEM	Ratio	Mutants	pEC50±SEM	Ratio	Mutants	pEC50±SEM	Ratio
WT	WT	7.30 ± 0.11	1	WT	7.90 ± 0.18	1	WT	8.16 ± 0.12	1
3x29				L115A	7.64 ± 0.25	-2	L99A	7.65 ± 0.13	-3
3x32	D116A	3.47 ± 0.27	-6761	D118A	3.88 ± 0.10	10520	D102A	KO	KO
3x33	V117A	5.74 ± 0.16	-36	I119A	6.39 ± 0.11	-33	M103A	7.71 ± 0.18	-3
3x33							M103S	7.74 ± 0.23	-3
3x36	C120A	4.68 ± 0.25	-417	C122A	6.62 ± 0.17	-19	C106A	7.59 ± 0.10	-4
3x37	T121A	5.28 ± 0.12	-105	T123A	5.32 ± 0.07	-382	T107A	6.9 ± 0.08	-18
5.38x39				Y197A	7.54 ± 0.18	-2			
5.42x43	S199A	6.20 ± 0.20	-13	S201A	7.48 ± 0.35	-3	S186A	7.7 ± 0.13	-3
5.43x44	T200A	6.23 ± 0.15	-12	T202A	7.04 ± 0.13	-7	T187A	7.49 ± 0.11	-5
5.46x461	A203F	KO	KO	A205F	4.60 ± 0.24	-1991	A190F	6.18 ± 0.05	-97
5.46x461	A203S	6.99 ± 0.10	-2	A205S	7.63 ± 0.16	-2	A190S	7.65 ± 0.11	-3
6x48				W314A	5.53 ± 0.47	-236	W304A	6.33 ± 0.12	-68
6x51	F361A	5.52 ± 0.28	-60	F317A	5.87 ± 0.14	-108	F307A	7.31 ± 0.06	-7
6x52	F362A	5.27 ± 0.19	-107	F318A	8.15 ± 0.22	1	F308A	7.63 ± 0.16	-3
6x55				S321A	7.43 ± 0.20	-3	E311A	7.18 ± 0.13	-10
6x55							E311S	7.03 ± 0.05	-14
7.39x38				T342	7.20 ± 0.12	-5	T330A	7.35 ± 0.08	-7
7.43x42	Y390A	6.30 ± 0.26	-10	Y346A	KO	KO	Y334A	6.46 ± 0.27	-50
7.43x42	Y390F	7.10 ± 0.14	-2	Y346F	KO	KO	Y334F	7.54 ± 0.20	-4
ECL2	I189A	5.31 ± 0.28	-98	N191A	8.04 ± 0.14	1	I175A	7.38 ± 0.19	-6

o^3

Extended Data Fig. 7. Ligand-binding pocket mutagenesis data by NanoBiT G_i-protein recruitment assay.

Data are shown as mean ± SEM from at least three independent experiments performed in technical triplicate. The EC_{50} ratio, EC_{50}(mutant)/EC_{50}(WT), represents the shift between the WT and mutant curves, and characterizes the effect of the mutations on receptor activation.

a

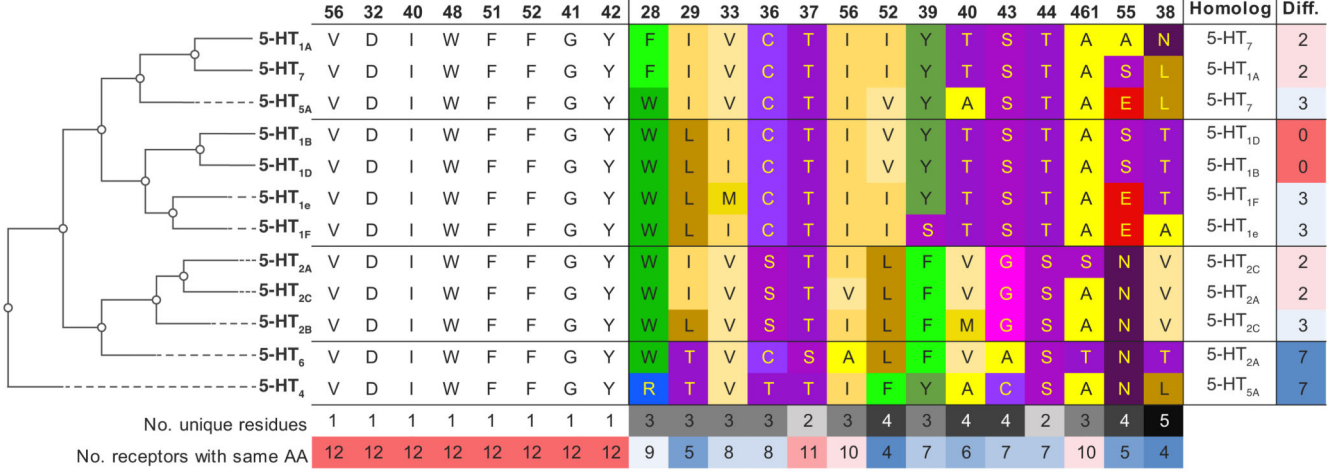

	Conserved								non-Conserved															Closest Homolog	No. Diff.
	2x 56	3x 32	3x 40	6x 48	6x 51	6x 52	7x 41	7x 42	3x 28	3x 29	3x 33	3x 36	3x 37	4x 56	45x 52	5x 39	5x 40	5x 43	5x 44	5x 461	6x 55	7x 38		
5-HT$_{1A}$	V	D	I	W	F	F	G	Y	F	I	V	C	T	I	I	Y	T	S	T	A	A	N	5-HT$_{7}$	2
5-HT$_{7}$	V	D	I	W	F	F	G	Y	F	I	V	C	T	I	I	Y	T	S	T	A	S	L	5-HT$_{1A}$	2
5-HT$_{5A}$	V	D	I	W	F	F	G	Y	W	I	V	C	T	I	V	Y	A	S	T	A	E	L	5-HT$_{7}$	3
5-HT$_{1B}$	V	D	I	W	F	F	G	Y	W	L	I	C	T	I	V	Y	T	S	T	A	S	T	5-HT$_{1D}$	0
5-HT$_{1D}$	V	D	I	W	F	F	G	Y	W	L	I	C	T	I	V	Y	T	S	T	A	S	T	5-HT$_{1B}$	0
5-HT$_{1e}$	V	D	I	W	F	F	G	Y	W	L	M	C	T	I	I	Y	T	S	T	A	E	T	5-HT$_{1F}$	3
5-HT$_{1F}$	V	D	I	W	F	F	G	Y	W	L	I	C	T	I	I	S	T	S	T	A	E	A	5-HT$_{1e}$	3
5-HT$_{2A}$	V	D	I	W	F	F	G	Y	W	I	V	S	T	I	L	F	V	G	S	S	N	V	5-HT$_{2C}$	2
5-HT$_{2C}$	V	D	I	W	F	F	G	Y	W	I	V	S	T	V	L	F	V	G	S	A	N	V	5-HT$_{2A}$	2
5-HT$_{2B}$	V	D	I	W	F	F	G	Y	W	L	V	S	T	I	L	F	M	G	S	A	N	V	5-HT$_{2C}$	3
5-HT$_{6}$	V	D	I	W	F	F	G	Y	W	T	V	C	S	A	L	F	V	A	S	T	N	T	5-HT$_{2A}$	7
5-HT$_{4}$	V	D	I	W	F	F	G	Y	R	T	V	T	T	I	F	Y	A	C	S	A	N	L	5-HT$_{5A}$	7
No. unique residues	1	1	1	1	1	1	1	1	3	3	3	3	2	3	4	3	4	4	2	3	4	5		
No. receptors with same AA	12	12	12	12	12	12	12	12	9	5	8	8	11	10	4	7	6	7	7	10	5	4		

b

Ligands	5-HT$_{5A}$	5-HT$_{7}$	5-HT$_{1A}$	5-HT$_{1B}$	5-HT$_{1D}$	5-HT$_{1e}$	5-HT$_{1F}$	5-HT$_{2A}$	5-HT$_{2B}$	5-HT$_{2C}$	5-HT$_{6}$	5-HT$_{4}$
5-CT	7.7	9.1	8.9	8.9	9.0	5.4	6.1	6.4	7.1	6.1	6.3	5.0
5-HT	6.9	8.1	8.4	8.4	8.5	8.2	7.3	7.1	8.4	7.9	7.1	6.6
5-MeOT		8.3		8.2	8.3	5.5	5.9	6.8	8.5	7.3	7.4	6.2
Aripiprazole	5.9	7.7	8.3	6.1	7.2	5.1		7.8	9.4	7.8	6.5	
BRL54443		5.0	7.2	6.9	7.2	8.7	8.9	5.9	7.0	6.5	5.0	
DHE		8.0	8.8	9.6	9.9				7.6		8.3	
Donitriptan	5.6		7.6	9.4	9.3	5.9	5.5	6.6				6.1
Ergotamine		5.9	9.8	8.3	9.0	6.6	6.8	9.1	8.4	8.4	7.9	
GR127935	5.2	5.6	7.1	8.9	8.8	5.4	6.4	7.6	6.2	7.0	5.4	
Risperidone	6.7	8.5	6.5	7.7	7.6	5.4	5.9	9.4	7.3	7.7	5.7	
Ritanserin		7.3	5.5	6.6	6.3			9.1	8.7	9.0	7.5	
Tryptamine		6.8	7.0	6.7	7.0	5.6	5.6	6.1	7.3	6.5	6.4	
Zotepine	7.5	8.1	6.4	7.2	7.0	6.2		8.6		8.5	8.6	

O^{3}

Extended Data Fig. 8. Serotonin binding pocket alignment and ligands affinity among serotonin receptors.

a, Dendrogram and sequence alignment based on residues lining the serotonin binding pocket (5 Å cut-off). Identical residues are marked in white, whereas non-conserved are colored by their physicochemical properties. **b,** binding affinities (pKi values) for selected ligands of the 5-HT receptors. (https://pdsp.unc.edu/pdspweb/)

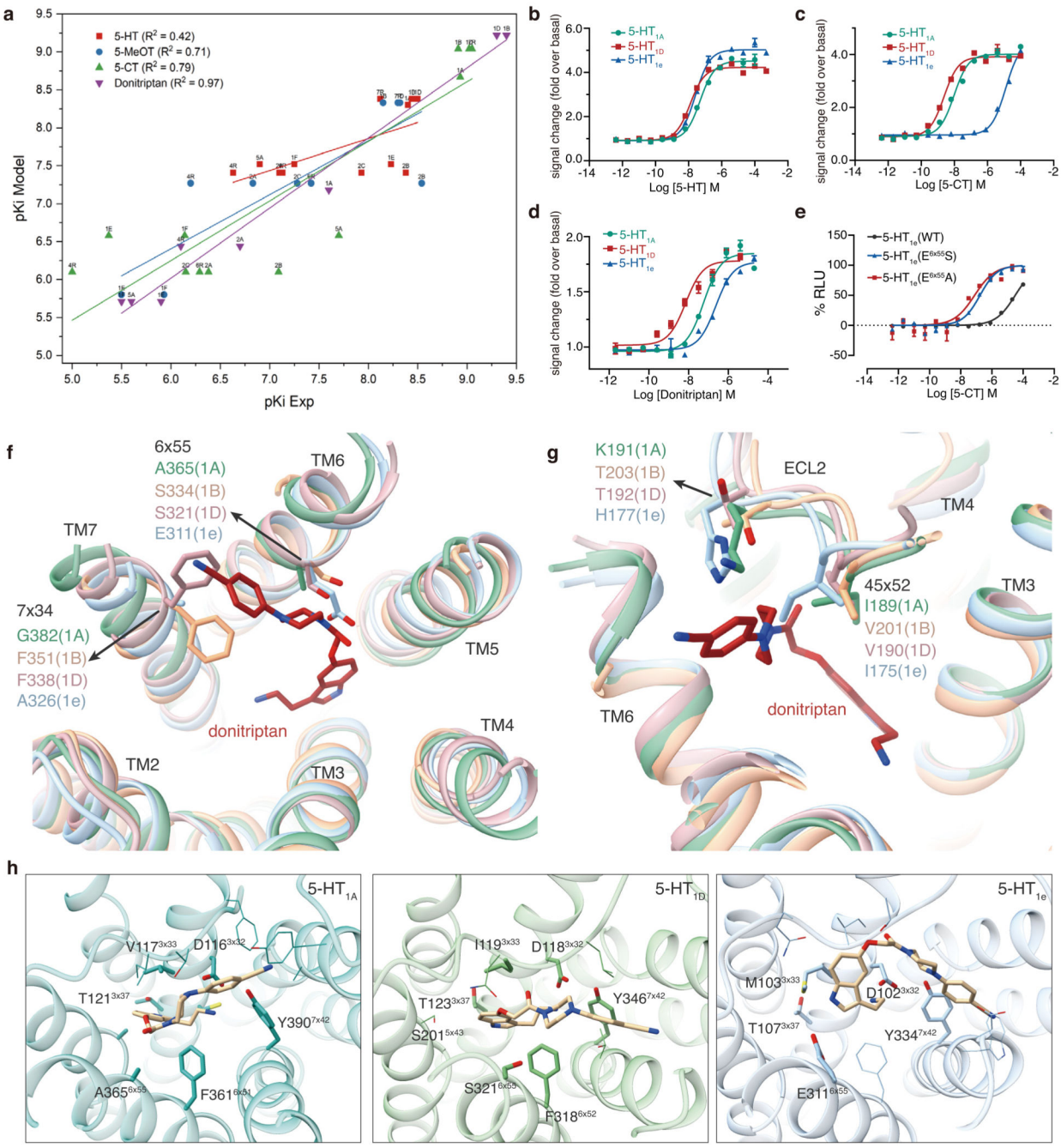

Extended Data Fig. 9. Selectivity of 5-HT$_1$ subfamily receptors.

a, Fitted regression model versus experimental binding affinities of 5-HT, 5-MeOT, 5-CT, and donitriptan for the GPCR 5-HT receptors. **b-d**, Serotonin- (**b**), 5-CT- (**c**), and donitriptan-(**d**) induced G_i activation assay using NanoBiT for wild type 5-HT$_{1A}$, 5-HT$_{1D}$, and 5-HT$_{1e}$ receptors. Data are shown as mean ± SEM from at least three independent experiments performed in technical triplicate. **e**, 5-CT-induced G_i activation assay using NanoBiT for 5-HT$_{1e}$, and concentration-response curves for G-protein recruitment signals. Data are shown as mean ± SEM from at least three independent experiments performed in

Europe PMC Funders Author Manuscripts

technical triplicate. **f**, **g**, The different side chains at TMD (**f**) and at ECL2 (**g**) that determine the recognition for donitriptan among 5-HT_{1A}, 5-HT_{1B}, 5-HT_{1D}, and 5-HT_{1e}. **h**, Docked pose of donitriptan in donitriptan-bound 5-HT_{1A} (right), 5-HT_{1D} (middle), and 5-HT_{1e} (left).

Extended Data Table 1

Cryo-EM data collection, refinement and validation statistics

	Apo–5-HT1A–Gi (EMD-30971) (PDB 7E2X)	5-HT–5-HT1A–Gi (EMD-30972) (PDB 7E2Y)	Aripiprazole–5-HT1A–Gi (EMD-30973) (PDB 7E2Z)	5-HT–5-HT1D–Gi–scFv16 (EMD-30974) (PDB 7E32)	BRL-54443–5-HT1e–Gi–scFv16 (EMD-30975) (PDB 7E33)
Data Collection and Processing					
Magnification	49,310	49,310	49,310	47,847	47,847
Voltage (kV)	300	300	300	300	300
Electron exposure (e-/Å2)	64	64	64	70	70
Defocus range (μm)	-1.0 ~ -3.0	-1.0 ~ -3.0	-1.0 ~ -3.0	-1.0 ~ -3.0	-1.0 ~ -3.0
Pixel size (Å)	1.014	1.014	1.014	1.045	1.045
Symmetry imposed	C1	C1	C1	C1	C1
Initial particle projections (no.)	2,719,825	5,279,538	1,486,169	4,212,737	4,977,538
Final particle projections (no.)	245,886	472,338	154,241	141,501	163,354
Map resolution (Å)	3.0	3.0	3.1	2.9	2.9
FSC threshold	0.143	0.143	0.143	0.143	0.143
Map resolution range (Å)	2.2-5	2.2-5	2.2-5	2.2-5	2.2-5
Refinement					
Initial model used (PDB code)	6G79, 6CMO	6G79, 6CMO	6G79, 6CMO	6G79, 6CMO	6G79, 6CMO
Model resolution (Å)	3.0	3.2	3.2	3.0	3.1
FSC threshold	0.5	0.5	0.5	0.5	0.5
Model resolution range (Å)	50-3.0	48-3.2	48-3.2	48-3.0	48-3.1
Map sharpening B factor (Å2)	-115.387	-108.16	-125.267	-88.65	-88.26
Model Composition Non-hydrogen atoms	7287	7035	7073	8839	8610
Protein residues	890	873	880	1116	1091
Lipids	15	5	6	1	1
B factors (Å2) Protein	160.4	100.4	55.5	118.5	115.6
Ligand	161.6	109.7	60.9	55.5	99.8

Europe PMC Funders Author Manuscripts

	Apo–5-HT1A–Gi (EMD-30971) (PDB 7E2X)	5-HT–5-HT1A–Gi (EMD-30972) (PDB 7E2Y)	Aripiprazole–5-HT1A–Gi (EMD-30973) (PDB 7E2Z)	5-HT–5-HT1D–Gi–scFv16 (EMD-30974) (PDB 7E32)	BRL-54443–5-HT1e–Gi–scFv16 (EMD-30975) (PDB 7E33)
R.m.s. deviations Bond lengths (Å)	0.005	0.005	0.005	0.017	0.006
Bond angles (°)	1.13	1.16	1.11	1.10	0.96
Validation					
MolProbity score	1.42	1.51	1.35	1.72	1.59
Clashscore	4.48	4.19	4.39	9.16	10.02
Poor rotamer (%)	0.00	0.00	0.00	0.00	0.11
Ramachandran Plot Favored (%)	96.9	95.6	97.3	96.4	97.7
Allowed (%)	3.1	4.4	2.7	3.6	2.3
Disallowed (%)	0.0	0.0	0.0	0.0	0.0

Supplementary Material

Refer to Web version on PubMed Central for supplementary material.

Acknowledgements

The cryo-EM data were collected at the Center of Cryo-Electron Microscopy, Zhejiang University, and at the Center of Cryo-Electron Microscopy, Shanghai Institute of Materia Medica. This work was partially supported by the National Key R&D Programs of China (2018YFA0507002), the Shanghai Municipal Science and Technology Major Project (2019SHZDZX02), the CAS Strategic Priority Research Program (XDB37030103) to H.E.X.; the National Key Basic Research Program of China (2019YFA0508800), the National Natural Science Foundation of China (81922071), the Zhejiang Province Natural Science Fund for Excellent Young Scholars (LR19H310001), Fundamental Research Funds for the Central Universities (2019XZZX001-01-06) to Y.Z.; the National Natural Science Foundation (31770796) and National Science and Technology Major Project (2018ZX09711002-002-002) to Y.J.; Fund of Youth Innovation Promotion Association (2018319 Y8G7011009) to X.C.; Science and Technology Commission of Shanghai Municipal (20431900100) and Jack Ma Foundation (2020-CMKYGG-05) to H.J.; the EU Horizon 2020, Innovative Training Network SAFER (765657) to I.A.S.; the Lundbeck Foundation (R163-2013-16327) and Novo Nordisk Foundation (NNF18OC0031226) to D.E.G. and K.H.; a Wellcome Trust Investigator Award (104633/Z/14/Z) to C.V.R. and H.-Y.Y.

Data and materials availability

Density maps and structure coordinates have been deposited to the Electron Microscopy Database (EMDB) and the Protein Data Bank (PDB) with the accession codes EMD-30971 and 7E2X for the apo–5-HT_{1A}–G_i complex; EMD-30972 and 7E2Y for the 5-HT–5-HT_{1A}–G_i complex; EMD-30973 and 7E2Z for the aripiprazole–5-HT_{1A}–G_i complex; EMD-30974 and 7E32 for the 5-HT–5-HT_{1D}–G_i complex; EMD-30975 and 7E33 for the 5-HT–5-HT_{1e}–G_i complex.

References

1. Berger M, Gray JA, Roth BL. The Expanded Biology of Serotonin. Annual Review of Medicine. 2009; 60:355–366. DOI: 10.1146/annurev.med.60.042307.110802
2. Mohammad-Zadeh LF, Moses L, Gwaltney-Brant SM. Serotonin: a review. J Vet Pharmacol Ther. 2008; 31:187–199. DOI: 10.1111/j.1365-2885.2008.00944.x [PubMed: 18471139]

3. Hannon J, Hoyer D. Molecular biology of 5-HT receptors. Behav Brain Res. 2008; 195:198–213. DOI: 10.1016/j.bbr.2008.03.020 [PubMed: 18571247]
4. Barnes NM, et al. International Union of Basic and Clinical Pharmacology. CX. Classification of Receptors for 5-hydroxytryptamine; Pharmacology and Function. Pharmacol Rev. 2021; 73:310–520. DOI: 10.1124/pr.118.015552 [PubMed: 33370241]
5. Dawaliby R, et al. Allosteric regulation of G protein-coupled receptor activity by phospholipids. Nat Chem Biol. 2016; 12:35.doi: 10.1038/Nchembio.1960 [PubMed: 26571351]
6. Duncan AL, Song WL, Sansom MSP. Lipid-Dependent Regulation of Ion Channels and G Protein-Coupled Receptors: Insights from Structures and Simulations. Annu Rev Pharmacol. 2020; 60:31–50. DOI: 10.1146/annurev-pharmtox-010919-023411
7. van Meer G, Voelker DR, Feigenson GW. Membrane lipids: where they are and how they behave. Nat Rev Mol Cell Bio. 2008; 9:112–124. DOI: 10.1038/nrm2330 [PubMed: 18216768]
8. Di Paolo G, De Camilli P. Phosphoinositides in cell regulation and membrane dynamics. Nature. 2006; 443:651–657. DOI: 10.1038/nature05185 [PubMed: 17035995]
9. de Rubio RG, et al. Phosphatidylinositol 4-phosphate is a major source of GPCR-stimulated phosphoinositide production. Sci Signal. 2018; 11doi: 10.1126/scisignal.aan1210
10. Yen HY, et al. PtdIns(4,5)P-2 stabilizes active states of GPCRs and enhances selectivity of G-protein coupling. Nature. 2018; 559:424.doi: 10.1038/s41586-018-0325-6
11. Falkenburger BH, Jensen JB, Dickson EJ, Suh BC, Hille B. Phosphoinositides: lipid regulators of membrane proteins. J Physiol-London. 2010; 588:3179–3185. DOI: 10.1113/jphysiol.2010.192153 [PubMed: 20519312]
12. Seifert R, Wenzel-Seifert K. Constitutive activity of G-protein-coupled receptors: cause of disease and common property of wild-type receptors. N-S Arch Pharmacol. 2002; 366:381–416. DOI: 10.1007/s00210-002-0588-0
13. Teitler M, Herrick-Davis K, Purohit A. Constitutive activity of G-protein coupled receptors: emphasis on serotonin receptors. Curr Top Med Chem. 2002; 2:529–538. DOI: 10.2174/1568026023393859 [PubMed: 12052192]
14. De Deurwaerdere P, Bharatiya R, Chagraoui A, Di Giovanni G. Constitutive activity of 5-HT receptors: Factual analysis. Neuropharmacology. 2020; 168:ARTN 107967.doi: 10.1016/j.neuropharm.2020.107967
15. Berg KA, Harvey JA, Spampinato U, Clarke WP. Physiological and therapeutic relevance of constitutive activity of 5-HT 2A and 5-HT 2C receptors for the treatment of depression. Prog Brain Res. 2008; 172:287–305. DOI: 10.1016/S0079-6123(08)00914-X [PubMed: 18772038]
16. Gutierrez MG, Mansfield KS, Malmstadt N. The Functional Activity of the Human Serotonin 5-HT1A Receptor Is Controlled by Lipid Bilayer Composition. Biophys J. 2016; 110:2486–2495. DOI: 10.1016/j.bpj.2016.04.042 [PubMed: 27276266]
17. Winner P. Triptans for migraine management in adolescents. Headache. 2002; 42:675–679. DOI: 10.1046/j.1526-4610.2002.02157.x [PubMed: 12482222]
18. Shimronabarbanell D, Nothen MM, Erdmann J, Propping P. Lack of Genetically-Determined Structural Variants of the Human Serotonin-1e (5-Ht1e) Receptor Protein Points to Its Evolutionary Conservation. Mol Brain Res. 1995; 29:387–390. DOI: 10.1016/0169-328x(95)00003-B [PubMed: 7609628]
19. Liang YL, et al. Dominant Negative G Proteins Enhance Formation and Purification of Agonist-GPCR-G Protein Complexes for Structure Determination. ACS Pharmacol Transl Sci. 2018; 1:12–20. DOI: 10.1021/acsptsci.8b00017 [PubMed: 32219201]
20. Yin W, et al. Crystal structure of the human 5-HT1B serotonin receptor bound to an inverse agonist. Cell Discov. 2018; 4:12.doi: 10.1038/s41421-018-0009-2 [PubMed: 29560272]
21. Garcia-Nafria J, Nehme R, Edwards PC, Tate CG. Cryo-EM structure of the serotonin 5-HT1B receptor coupled to heterotrimeric Go. Nature. 2018; 558:620–623. DOI: 10.1038/s41586-018-0241-9 [PubMed: 29925951]
22. Carlson ML, et al. The Peptidisc, a simple method for stabilizing membrane proteins in detergent-free solution. Elife. 2018; 7doi: 10.7554/eLife.34085

23. Evans KL J, Cropper JD, Berg KA, Clarke WP. Mechanisms of regulation of agonist efficacy at the 5-HT1A receptor by phospholipid-derived signaling components. J Pharmacol Exp Ther. 2001; 297:1025–1035. [PubMed: 11356925]
24. Pucadyil TJ, Chattopadhyay A. Cholesterol modulates the antagonist-binding function of hippocampal serotonin(1A) receptors. Bba-Biomembranes. 2005; 1714:35–42. DOI: 10.1016/j.bbamem.2005.06.005 [PubMed: 16005846]
25. Kim K, et al. Structure of a hallucinogen-activated gq-coupled 5-ht2a serotonin receptor. Cell. 2020; 182:1574–1588.e1519. [PubMed: 32946782]
26. Forster EA, et al. A Pharmacological Profile of the Selective Silent 5-Ht1a Receptor Antagonist, Way-100635. Eur J Pharmacol. 1995; 281:81–88. DOI: 10.1016/0014-2999(95)00234-C [PubMed: 8566121]
27. Zhou QT, et al. Common activation mechanism of class A GPCRs. Elife. 2019; 8:ARTN e50279.doi: 10.7554/eLife.50279
28. Pandy-Szekeres G, et al. GPCRdb in 2018: adding GPCR structure models and ligands. Nucleic Acids Res. 2018; 46:D440–D446. DOI: 10.1093/nar/gkx1109 [PubMed: 29155946]
29. Klein MT, Dukat M, Glennon RA, Teitler M. Toward Selective Drug Development for the Human 5-Hydroxytryptamine 1E Receptor: A Comparison of 5-Hydroxytryptamine 1E and 1F Receptor Structure-Affinity Relationships. J Pharmacol Exp Ther. 2011; 337:860–867. DOI: 10.1124/jpet.111.179606 [PubMed: 21422162]
30. Xu P, et al. Structures of the human dopamine D3 receptor-Gi complexes. Molecular Cell. 2021
31. Davies MA, Sheffler DJ, Roth BL. Aripiprazole: a novel atypical antipsychotic drug with a uniquely robust pharmacology. CNS Drug Rev. 2004; 10:317–336. DOI: 10.1111/j.1527-3458.2004.tb00030.x [PubMed: 15592581]
32. Sjogren B, Csoregh L, Svenningsson P. Cholesterol reduction attenuates 5-HT1A receptor-mediated signaling in human primary neuronal cultures. Naunyn Schmiedebergs Arch Pharmacol. 2008; 378:441–446. DOI: 10.1007/s00210-008-0323-6 [PubMed: 18607571]
33. Chun E, et al. Fusion partner toolchest for the stabilization and crystallization of G protein-coupled receptors. Structure. 2012; 20:967–976. DOI: 10.1016/j.str.2012.04.010 [PubMed: 22681902]
34. Wang C, et al. Structural Basis for Molecular Recognition at Serotonin Receptors. Science. 2013; 340:610–614. DOI: 10.1126/science.1232807 [PubMed: 23519210]
35. Roth CB, Hanson MA, Stevens RC. Stabilization of the human β 2-adrenergic receptor TM4–TM3–TM5 helix interface by mutagenesis of Glu1223. 41, a critical residue in GPCR structure. Journal of molecular biology. 2008; 376:1305–1319. [PubMed: 18222471]
36. Maeda S, et al. Development of an antibody fragment that stabilizes GPCR/G-protein complexes. Nat Commun. 2018; 9:3712.doi: 10.1038/s41467-018-06002-w [PubMed: 30213947]
37. Angiulli G, et al. New approach for membrane protein reconstitution into peptidiscs and basis for their adaptability to different proteins. Elife. 2020; 9:e53530. [PubMed: 32125274]
38. Zheng SQ, et al. MotionCor2: anisotropic correction of beam-induced motion for improved cryo-electron microscopy. Nat Methods. 2017; 14:331–332. DOI: 10.1038/nmeth.4193 [PubMed: 28250466]
39. Zhang K. Gctf: Real-time CTF determination and correction. J Struct Biol. 2016; 193:1–12. DOI: 10.1016/j.jsb.2015.11.003 [PubMed: 26592709]
40. Scheres SH. RELION: implementation of a Bayesian approach to cryo-EM structure determination. J Struct Biol. 2012; 180:519–530. DOI: 10.1016/j.jsb.2012.09.006 [PubMed: 23000701]
41. Kato HE, et al. Conformational transitions of a neurotensin receptor 1-Gi1 complex. Nature. 2019; 572:80–85. DOI: 10.1038/s41586-019-1337-6 [PubMed: 31243364]
42. Heymann JB. Guidelines for using Bsoft for high resolution reconstruction and validation of biomolecular structures from electron micrographs. Protein Sci. 2018; 27:159–171. DOI: 10.1002/pro.3293 [PubMed: 28891250]
43. Kang YY, et al. Cryo-EM structure of human rhodopsin bound to an inhibitory G protein. Nature. 2018; 558:553.doi: 10.1038/s41586-018-0215-y [PubMed: 29899450]
44. Pettersen EF, et al. UCSF Chimera--a visualization system for exploratory research and analysis. J Comput Chem. 2004; 25:1605–1612. DOI: 10.1002/jcc.20084 [PubMed: 15264254]

45. Emsley P, Cowtan K. Coot: model-building tools for molecular graphics. Acta Crystallogr D. 2004; 60:2126–2132. DOI: 10.1107/S0907444904019158 [PubMed: 15572765]
46. Croll TI. ISOLDE: a physically realistic environment for model building into low-resolution electron-density maps. Acta Crystallographica Section D: Structural Biology. 2018; 74:519–530. [PubMed: 29872003]
47. Adams PD, et al. PHENIX: a comprehensive Python-based system for macromolecular structure solution. Acta Crystallogr D Biol Crystallogr. 2010; 66:213–221. DOI: 10.1107/S0907444909052925 [PubMed: 20124702]
48. Williams CJ, et al. MolProbity: More and better reference data for improved all-atom structure validation. Protein Sci. 2018; 27:293–315. DOI: 10.1002/pro.3330 [PubMed: 29067766]
49. Pettersen EF, et al. UCSF ChimeraX: Structure visualization for researchers, educators, and developers. Protein Sci. 2021; 30:70–82. [PubMed: 32881101]
50. Halgren T, Murphy R, Friesner R, Beard H, Frye LW, Thomas Pollard A, Banks JL. Glide: A new approach for rapid, accurate docking and scoring. 2004; 2:1750–1759.
51. Sali A, Blundell TL. Comparative protein modelling by satisfaction of spatial restraints. J Mol Biol. 1993; 234:779–815. DOI: 10.1006/jmbi.1993.1626 [PubMed: 8254673]
52. Wu EL, et al. CHARMM-GUI Membrane Builder toward realistic biological membrane simulations. J Comput Chem. 2014; 35:1997–2004. DOI: 10.1002/jcc.23702 [PubMed: 25130509]
53. Guvench O, et al. CHARMM additive all-atom force field for carbohydrate derivatives and its utility in polysaccharide and carbohydrate-protein modeling. J Chem Theory Comput. 2011; 7:3162–3180. DOI: 10.1021/ct200328p [PubMed: 22125473]
54. MacKerell AD, et al. All-atom empirical potential for molecular modeling and dynamics studies of proteins. J Phys Chem B. 1998; 102:3586–3616. DOI: 10.1021/jp973084f [PubMed: 24889800]
55. Van Der Spoel D, et al. GROMACS: fast, flexible, and free. J Comput Chem. 2005; 26:1701–1718. DOI: 10.1002/jcc.20291 [PubMed: 16211538]
56. Hess B, Kutzner C, van der Spoel D, Lindahl E. GROMACS 4: Algorithms for Highly Efficient, Load-Balanced, and Scalable Molecular Simulation. J Chem Theory Comput. 2008; 4:435–447. DOI: 10.1021/ct700301q [PubMed: 26620784]
57. Bussi G, Donadio D, Parrinello M. Canonical sampling through velocity rescaling. The Journal of chemical physics. 2007; 126:014101. [PubMed: 17212484]
58. Aoki KM, Yonezawa F. Constant-pressure molecular-dynamics simulations of the crystal-smectic transition in systems of soft parallel spherocylinders. Phys Rev A. 1992; 46:6541–6549. DOI: 10.1103/physreva.46.6541 [PubMed: 9907963]
59. Hess B. P-LINCS: A Parallel Linear Constraint Solver for Molecular Simulation. J Chem Theory Comput. 2008; 4:116–122. DOI: 10.1021/ct700200b [PubMed: 26619985]

Europe PMC Funders Author Manuscripts

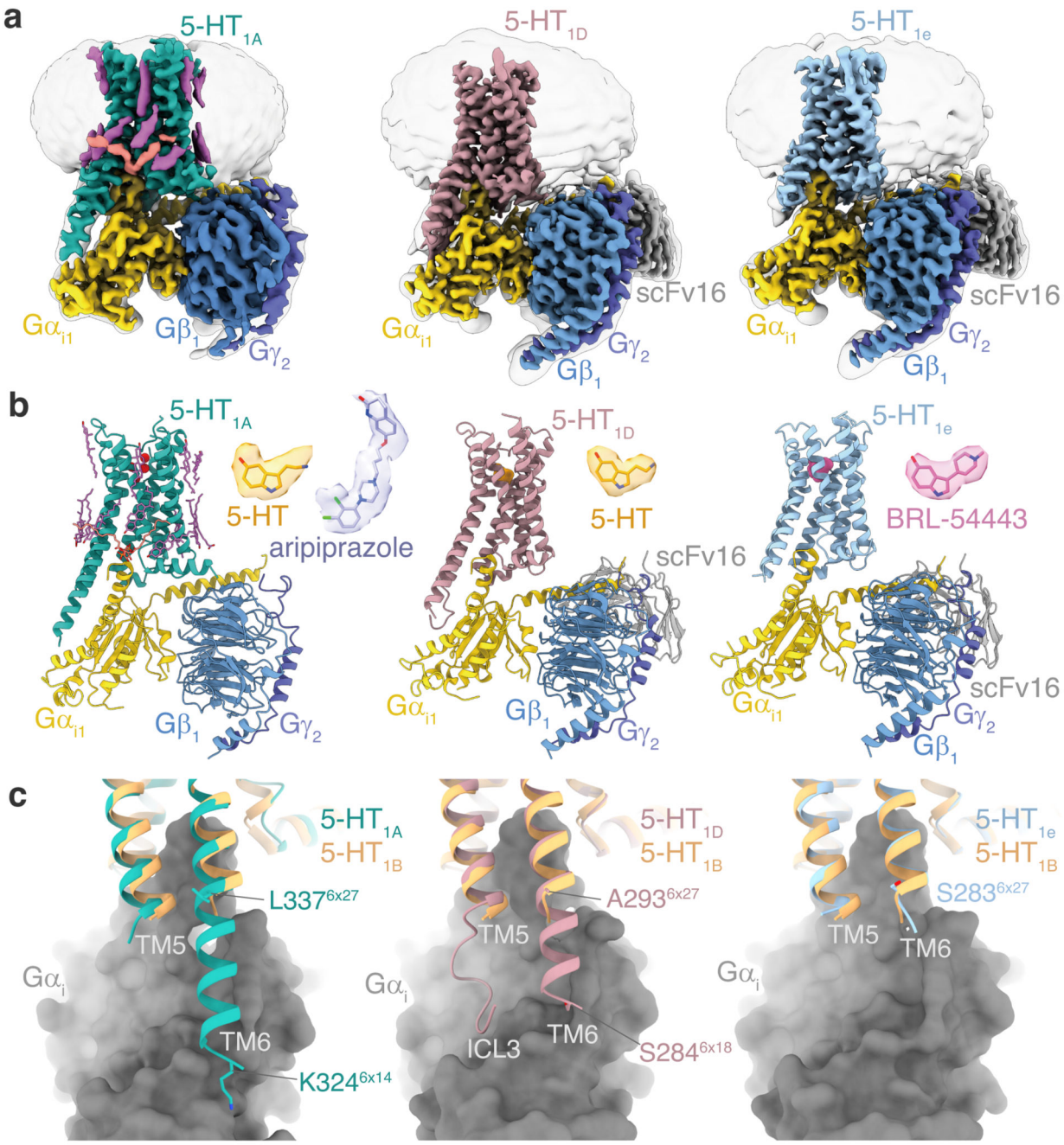

Fig. 1. Cryo-EM structures of the 5-HT$_{1A}$–G$_i$ complex, the 5-HT$_{1D}$–G$_i$ complex, and 5-HT$_{1e}$–G$_i$ complex.

a&b, Cryo-EM maps and structural models of the Gi complex of 5-HT$_{1A}$, 5-HT$_{1D}$, and 5-HT$_{1e}$. Ligands are shown at right side of the complexes with surrounding density maps. **c**, Comparison of the ICL3 of 5-HT$_{1B}$ with 5-HT$_{1A}$, 5-HT$_{1D}$, and 5-HT$_{1e}$.

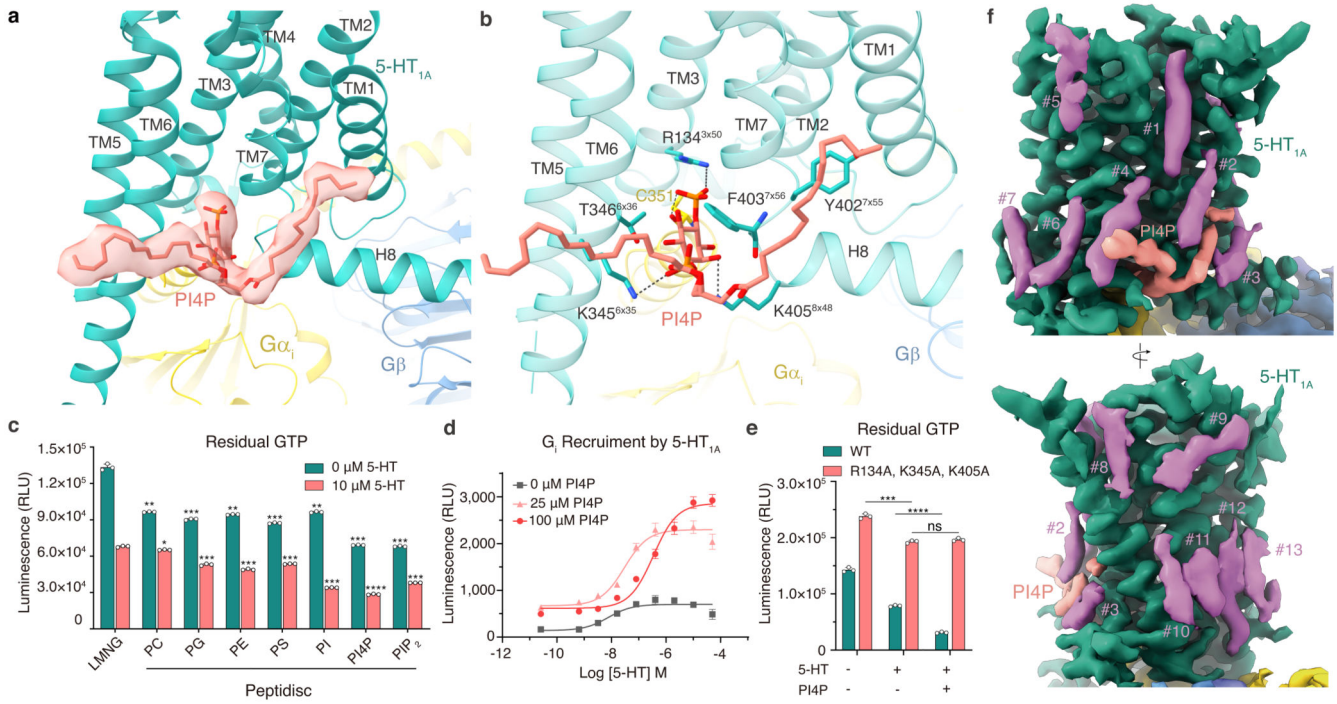

Fig. 2. Regulation of 5-HT$_{1A}$ by PI4P and cholesterol.

a, The bound PI4P at the interface between 5-HT$_{1A}$ and G$_i$ protein. PI4P is shown in red sticks with a surrounding density map at threshold 0.02. **b**, Interactions of PI4P at the 5-HT$_{1A}$–G$_i$ interface with interacting residues shown in sticks. Hydrogen bonds are shown with dashed lines. **c**, Receptor activation as measured by GTPase-Glo assay for different lipid-containing 5-HT$_{1A}$–G$_i$ peptidisc. Lower levels of residual GTP indicates higher levels of G protein activity upon receptor-mediated GDP/GTP exchange. The activation of 5-HT$_{1A}$ in different lipid-containing peptidisc was compared with that in LMNG micelle in the presence or absence of 5-HT. **d**, PI4P regulates 5-HT$_{1A}$ as a positive allosteric modulator. The G protein recruitment signal was detected by NanoBiT assay. Data are presented as mean ± SEM of three independent experiments performed in triplicate. **e**, Mutations on PI4P binding residues R134A, K345A, and K405A reduced the 5-HT$_{1A}$-mediated G-protein activation and abolished the regulation of PI4P. Data in panels **c**-**e** are presented as mean ± SD of three independent experiments performed in technical triplicate. *p < 0.05; **p < 0.01; ***p < 0.001; ****p < 0.0001; ns, no significance; two-tailed paired t-tests. **f**, Cryo-EM map of the apo 5-HT$_{1A}$ and the surrounding lipids. The densities of the 5-HT$_{1A}$ (green), cholesterol or fatty acids (purple), and PI4P (red) are colored with a 0.027 threshold.

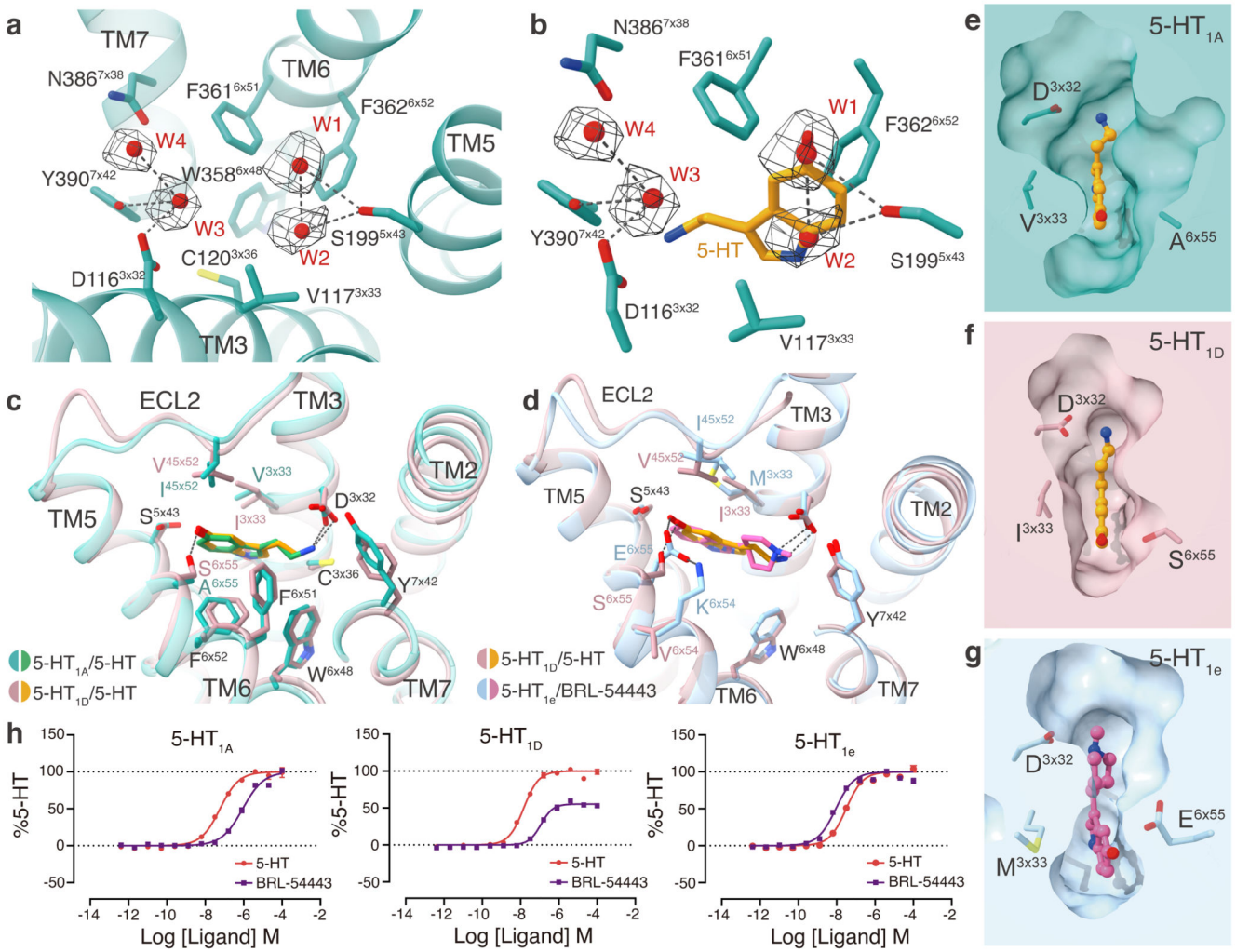

Fig. 3. The structure of waters in the apo 5-HT$_{1A}$ pocket and comparison between 5-HT and BRL-54443 structures.

a, Waters in the apo 5-HT$_{1A}$ ligand binding pocket with EM maps of waters shown in mesh. Hydrogen bonds are shown with dashed lines. **b**, Superposition of 5-HT and waters in the structures of the 5-HT$_{1A}$–G$_i$ complexes. **c**, Comparison of 5-HT recognition between 5-HT$_{1A}$ and 5-HT$_{1D}$. **d**, Comparison of ligand recognition between 5-HT bound 5-HT$_{1D}$ and BRL-54443 bound 5-HT$_{1e}$. **e-g**, The difference in the orthosteric binding pockets among 5-HT$_{1A}$ (e), 5-HT$_{1D}$ (**f**), and 5-HT$_{1e}$ (**g**). **h**. Concentration-response curves of 5-HT$_{1A}$, 5-HT$_{1D}$, and 5-HT$_{1e}$ activation by 5-HT and BRL-54443. Data are presented as mean ± SEM of three independent experiments performed in triplicate.

Europe PMC Funders Author Manuscripts

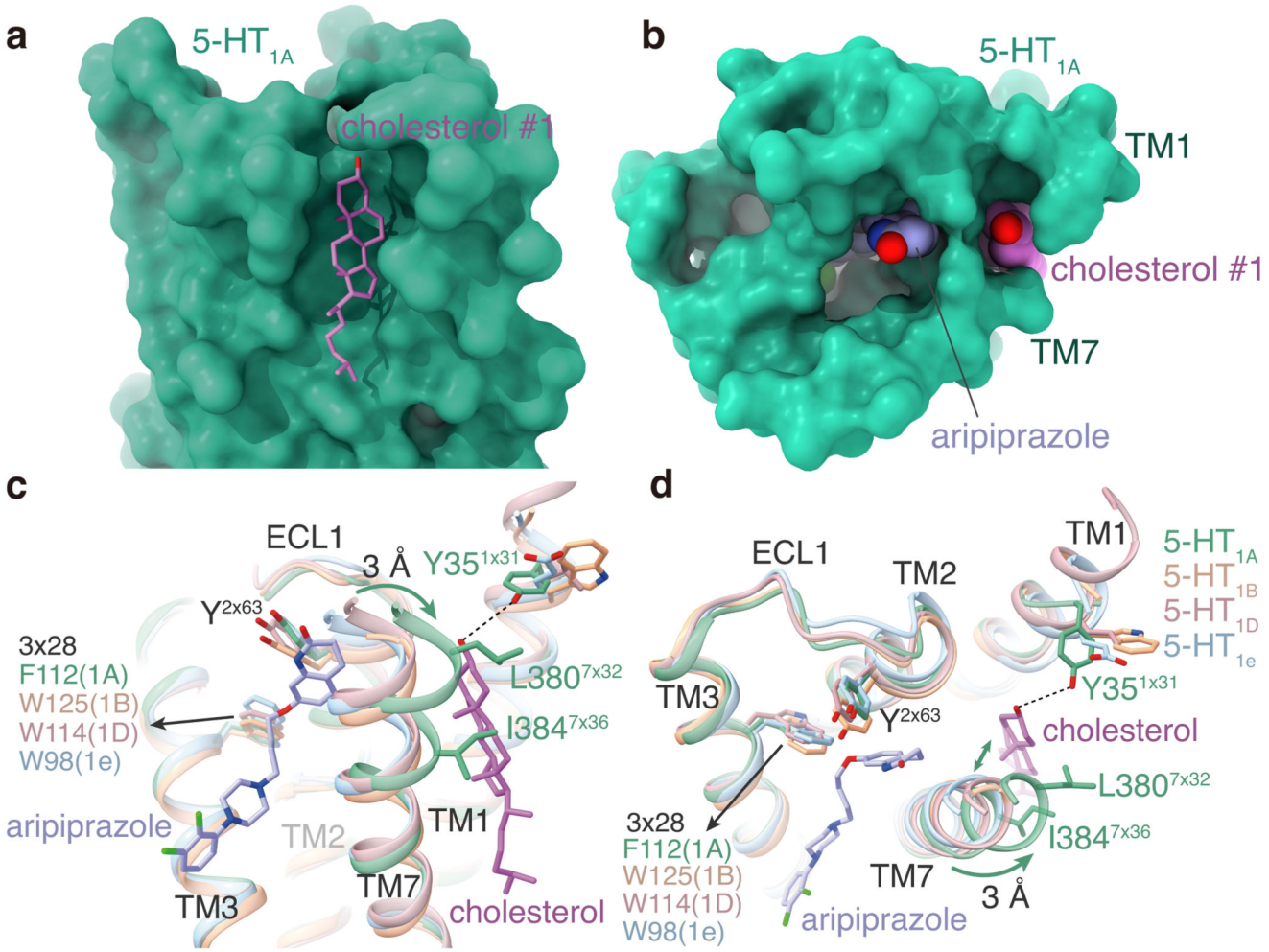

Fig. 4. The binding of aripiprazole is regulated by cholesterol.

a, A cholesterol at the surface between TM1 and TM7 of 5-HT_{1A}. **b**, Top view of aripiprazole bound 5-HT_{1A} structure. The 5-HT_{1A} is shown in surface. **c**, **d**, Differences in the conformation of TM7 and its interaction with aripiprazole and cholesterol in 5-HT_{1A} from 5-HT_{1B} (6G79), 5-HT_{1D} and 5-HT_{1e}.